MODELING AND ANALYSIS OF HEAT TRANSFER IN A FOUR-SEASON GREENHOUSE USING ANSYS FLUENT CFD SOFTWARE

By

© Amir Khoshbooie

A Thesis submitted to the School of Graduate Studies as partial fulfillment of the requirements for the degree of

MSc in Physics

Department of Physics and Physical Oceanography

Faculty of Science

Memorial University of Newfoundland

December 2024

St. John's Newfoundland

Abstract

In multiseason greenhouses, heating and cooling systems account for a significant part of the total operating cost. To make greenhouses more efficient it is important to reduce their reliance on external sources of energy as well as to minimize the energy wasted when it is most available. To do this a ground to air heat transfer (GAHT) system is used to store excess heat available during the daytime into the ground where it can be recovered during the night when the temperature in the greenhouse decreases to sub optimum levels. In this work, the mixture multiphase model in ANSYS Fluent was used to model and analyze the flow and energy exchange of dry and humid air through a simple GAHT system during daytime and nighttime conditions.

The analysis of the dry air at initially 35 °C showed that approximately 70 kJ of heat stored in the air was able to be transferred to the cold soil initially at 15 °C and that increasing the flow of the air caused the exchange in heat to occur faster. The analysis of air initially at 35 °C with 80% relative humidity was able to transfer between 400 and 450 kJ of energy to the ground initially at 15 °C. This exchange of heat occurred predominantly due to thermal contact between the air and the soil/GAHT system and through the latent heat of condensation resulting in approximately a factor of 6 increase in energy exchange compared to dry air. In the last part of this work, we simulated nighttime conditions where colder air initially at 5 °C with 50% relative humidity was forced to circulate in the GAHT system with the ground initially at 15 °C. The results showed that the ground was able to successful transfer energy to the air warming the latter to 16 °C. In this case the exchange

of thermal energy was significantly less with heat being transferred from the ground to the air, from the latent heat of condensation to the ground, and finally from the thermal energy of the air back to the ground.

The results of this work demonstrated great potential for using ANSYS Fluent to further study the design characteristics of GAHT systems in the hopes of increasing their efficiency.

Acknowledgements

First and foremost, I express my appreciation to my supervisor Dr. Luc Beaulieu for giving me the opportunity to work on this project and providing me with endless support, encouragement and guidance throughout my program. Without his patience, advice and contributions, the completion of this thesis would not have been possible.

I thank my parents for their support and encouragement and also my brother and sister who provided me with endless love and understanding as I went through this journey.

Simulations in this work were conducted on Digital Research Alliance of Canada [formerly Compute Canada] computing clusters and I thank them for providing us with computational resources and technical supports.

For those who are not mentioned here, your support is appreciated, and your contribution will never be forgotten.

Table of Contents

Abstract ……... ii

Acknowledgements ……...…. iv

List of Figures ……..……... ix

List of Tables …….. xi

List of Symbols and Abbreviations …….. xii

Chapter 1 Introduction ……. 1

1.1 Background ……... 1

1.2 A Historical Perspective …… 2

1.3 The Need for Four-season Greenhouse ……. 8

1.4 Statement of the Problem …… 10

1.5 Objectives ……..... 10

1.6 Thesis Outline ……. 11

Chapter 2 Literature Review ……. 12

2.1 Greenhouse Design ……. 12

2.2 Covering Material …… 13

2.2.1 Radiometric Properties ……. 13

2.2.2 Thermal Properties …….. 15

2.2.3 Mechanical Properties …….. 17

2.2.3.1 Loading Conditions ……... 18

2.2.3.2 Structural Design …….. 19

2.2.3.3 Installation …… 20

2.2.3.4 Environmental Effects …….. 22

2.3 Shape …….. 24

2.4 Orientation …….. 26

2.5 Climate Control …….. 26

2.5.1 Mathematical Modeling ……... 27

2.5.2 Computational Fluid Dynamics ……... 28

Chapter 3 An Introduction to ANSYS Fluent ……... 33

3.1 Definition of CFD ……... 33

3.2 CFD Code Structure …… 33

3.2.1 Pre-processor ……... 34

3.2.2 Solver …….. 35

3.2.3 Post-processor …… 38

3.3 ANSYS Fluent ……... 39

3.3.1 Getting Started …… 39

3.3.2 Geometry …… 41

3.3.3 Mesh …… 43

3.3.4 Solver …… 46

3.3.4.1 Setup …… 47

3.3.4.2 Solution …… 48

3.3.5 Results …… 50

3.4 Models Investigated in This Work …… 52

3.4.1 General Description of The Model …… 53

3.4.2 Soil as A Porous Medium …… 54

3.4.3 Surface Condensation with Eulerain Wall Film Model …… 55

3.4.4 Phase Change Using Mixture Multiphase Model …… 60

Chapter 4 Our Simulation Settings and The Results …… 65

4.1 Geometry …… 65

4.2 Mesh …… 66

4.3 Setup …… 68

4.4 Results …… 70

4.4.1 Dry Air …… 70

4.4.2 Humid Air 75

4.4.2.1 Hot Humid Air and Cold Soil 75

4.4.2.2 Cold Humid Air and Hot Soil 85

Chapter 5 Conclusion and Potential for Future Research 94

5.1 Conclusions 94

5.2 Suggestions for Future Works 97

5.2.1 Initial Conditions 97

5.2.2 Regarding the External Factors 97

5.2.3 Regarding the Internal Factors 98

5.2.4 Regarding the Geometry Design 99

References 101

Appendix A..... 107

List of Figures

Figure 1.1: Sectional view of a Korean greenhouse illustrates components of its design: thick walls for insulation, underfloor heating system known as “ondol”, a fireplace and caludron for boiling water enabling moisture control and chimney for fume exhaust [4]... 3

Figure 1.2: Using decomposition of manure to provide the heat in a greenhouse. This method was replaced by hydraulic heating systems after 1870 [5]……..... 5

Figure 1.3 Classification of greenhouse systems [2]..…….. 7

Figure 2.1: Greenhouse design components. Reproduced with permission from [8] 12

Figure 2.2: Illustration of clamps used for the purpose of securing the plastic films to the greenhouse structural parts; a) simple clip b) welded film. Acquired with permission from [9] 22

Figure 2.3: Five most frequently used shapes of greenhouses. Acquired with permission from [11] ...…… 24

Figure 3.1: A view of ANSYS workbench. ……... 39

Figure 3.2: A typical Fluent project consists of five components: Geometry, Mesh, Setup, Solution and Results, which must be completed in order. ……..... 40

Figure 3.3: A view of an illustrative DesignModeler project. ……... 43

Figure 3.4: A view of the meshing window. …….. 44

Figure 3.5: (a) Aspect Ratio of a cell zone. (b) Orthogonal Quality [32]……..... 45

Figure 3.6: A view of a Fluent window. …… 47

Figure 3.7: User gets notified when the solution is converged. ……. 50

Figure 3.8: A view of Results window, used for post-processing of a Fluent project.….... 51

Figure 3.9: Geometry of the model; a) 2D, b) 3D. ……. 53

Figure 3.10: A “porous zone” tab in a Fluent project. ……... 56

Figure 3.11: Eulerian Wall Film settings window. …… 59

Figure 3.12: Mixture multiphase model settings window. ……. 62

Figure 3.13: Phase interaction settings window in Mixture multiphase model.……. 64

Figure 4.1: Geometry of the computational domain used in this work. A square with sides 2 meters in length represents the greenhouse chamber while beneath is a rectangle 2 meters in length and 1 meter in depth which represents the soil domain. A 2D pipe with a wall

thickness of 1 millimeter and a diameter of 15 centimeters enters the soil on one side and exits from the other side. ...……. 66

Figure 4.2: Meshed computational domain, a) at the area when the pipe exits the soil and enters the chamber, b) at area inside the soil where pipe is bent……..……...67

Figure 4.3: Average temperature of a) dry air, and b) the solid....…… 73

Figure 4.4: a) The change in energy of the soil for the three fan pressures (30 Pa (red), 60 Pa (blue), 120 Pa (green)). …..…….. 75

Figure 4.5: a) Changes of air mixture temperature over time, b) changes of soil temperature over time, c) mass of liquid water over time (solid lines, left ordinate) and rate of change in liquid water production over time (solid lines with dots ⊸ right ordinate)....…… 79

Figure 4.6: a) The change in energy of the soil for the three fan pressures (30 Pa (red), 60 Pa (blue), 120 Pa (green))……...83

Figure 4.7: Changes in air average RH over time……... 84

Figure 4.8: a) Changes of air mixture temperature over time. b) Changes of soil temperature over time. c) Mass of liquid water over time (left) and rate of change in liquid water production over time (right)……..……. 88

Figure 4.9: a) The change in energy of the soil for the three fan pressures (30 Pa (red), 60 Pa (blue), 120 Pa (green))……..… 92

Figure 4.10: Changes in air average RH over time……..……... 93

Figure 5.1: Map of temperature distribution at t = 30s during the circulation of hot humid air (initially at 35 °C and 80% RH) through the cold soil (initially at 5 °C) at 30Pa fan pressure jump……100

List of Tables

Table 3.1: Comparison of spectral, finite element, and finite difference methods [38]…36

Table 4.1: Results of simulations conducted when hot dry air initially set to 35°C was circulated through a pipe surrounded by soil with an initial temperature of 15°C for 100s. ……... 70

Table 4.2: Results of simulations conducted when hot humid air initially set to 35°C and 80% RH was circulated through a pipe surrounded by soil with an initial temperature of 15°C for 600s. ……... 77

Table 4.3: Results of simulations conducted when colder humid air initially set to 5°C and 50% RH was circulated through a pipe surrounded by soil with an initial temperature of around 15°C for 200s.…… 85

List of Symbols and Abbreviations

CFD: Computational Fluid Dynamics

$\tau(\lambda)$: Spectral transmissivity

λ: wavelength

τ_s: solar transmissivity coefficient

$P_s(\lambda)$: wavelength distribution density function

$\rho(\lambda)$: spectral reflectivity

α: average solar absorption coefficient

ε: emissivity coefficient

k : coefficient of thermal conductivity

Q : heat flux through the sample

L : the sample thickness

A : the area of the sample

T_c : temperature of cold side

T_h : temperature of hot side

h : coefficient of convective heat transfer

h_h : coefficient of convective heat transfer for hot surface

h_c : coefficient of convective heat transfer for cold surface

K : overall coefficient of heat transfer

d_j : thickness of the j^{th} element

k_j : coefficient of thermal conductivity

u : maximum bending deflection of the gutters

L : distance between the rafters/trusses

n : number of panels

PVC : Polyvinyl Chloride

UV : Ultraviolet

HALS : Hindered Amide Light Stabilizers

PE : Polyethylene

Ni : Nickel

Φ **:** A general field variable of the flow

TDMA : Tri-Diagonal Matrix Algorithm

SIMPLE : Semi-Implicit Method for Pressure Linked Equations

SIMPLEC : Semi-Implicit Method for Pressure Linked Equations-Consistent

PISO : Pressure-Implicit with Splitting of Operators

PRESTO! : PREssure STaggering Option

QUICK : Quadratic Upstream Interpolation for Convective Kinematics

MUSCL : Monotonic Upstream-centered Scheme for Conservation Laws

GAHT : Ground to Air Heat Transfer

VOF : Volume of Fluid

EWF : Eulerian Wall Film

UDF : User Defined Function

LES : Large Eddy Simulation

MRF : Multiple Reference Frames

DPM : Discrete Phase Model

SST : Shear Stress Transport

RH : Relative Humidity

C_p : Specific Heat

k_B : Boltzmann Constant

E_T : Thermal Energy

N : Number of Molecules

Chapter 1 Introduction

1.1 Background

Agriculture and the cultivation of crops have had a crucial impact on civilization, not only for providing humans with the essential energy source, but also for paving the way for a transition from smaller nomadic hunter gatherers to larger settled societies. The ability to grow food and to maintain the energy supply has had and will continue to have great importance on both large-industrial and small-personal scales. One of the key factors in the process of cultivating plants is to reach and maintain the suitable growing conditions for enabling highly efficient and sustainable production. The desirable conditions for plants to grow may not be naturally available in many areas, especially those with harsh climates, and that is where the need to design and construct multi-season greenhouses emerges.

A greenhouse is a form of protected cultivation which provides some level of control over the growing conditions of crops, e.g. temperature, humidity, solar radiation intensity, etc. In this specialized form of agriculture, a variety of tools and technologies are utilized in order to create and maintain a stable environment which meets the criteria for the production of high-quality crops (vegetables, fruits, flowers, etc.) for prolonged periods of time in areas which naturally lack such conditions [1].

1.2 A Historical Perspective

As mentioned in the previous section, agriculture is as old as civilization, but it is not clear yet where in the history humans began to provide their plants and crops with types of artificial coverage and shielding with the purpose of protecting them against natural threats and enhancing the production. According to Lemmon (1962), who recorded the writings of ancient Greek philosopher Plato (427 – 328 B.C.), there is indication of plants growing under cover in one of Plato's writings, which can be considered as one the earliest and simplest attempts to provide protection for plants [2]. Another early instance of such practice can be tracked back to the Roman times, where during the era of emperor Tiberius (14 – 37 A.C.), cucumbers, and possibly other types of vegetables and/or fruits, were grown on portable beds. In sunny days, the beds were manually lifted and moved out under the sunlight, and in cold nights, they were sheltered in protected areas which had thin sheets of mica as roof [1].

One of the first instances of utilizing glass in the construction of protective structure for the plants has been in the year of 1385 in the Bois de Duc in France, where the glass pavilions facing towards the south were used as planting site for growing flowers. There have also been reports of structures with opaque roofs and glass side walls in Apothecaries Garden, Chelsea, England around the same time [2]. In the 15th century in Korea, cold frames which allowed some levels of management and control over the temperature and humidity of the crops were used. In these structures, manure or other types of organic matter were burnt as fuel and an iron pot containing boiling water would enable moisture regulation (Figure 1.1).

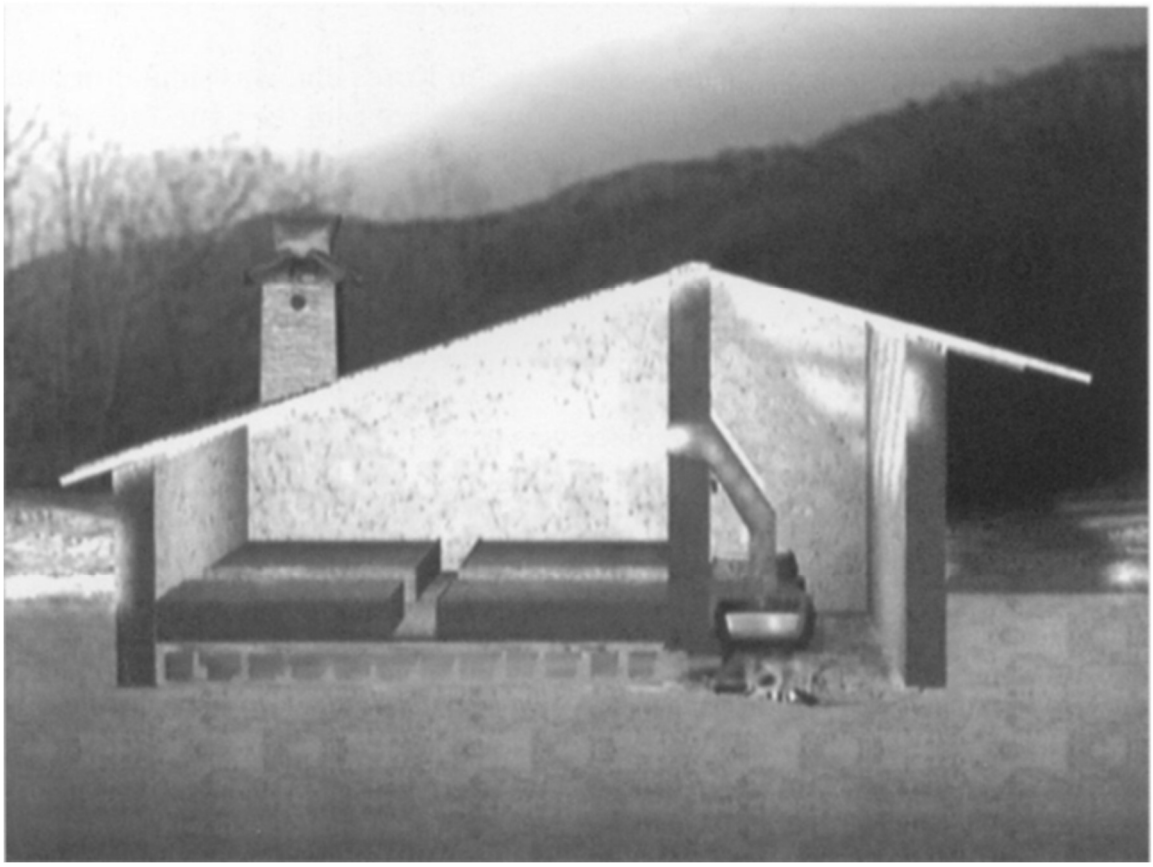

Figure 1.1: Sectional view of a Korean greenhouse illustrates components of its design: thick walls for insulation, underfloor heating system known as "ondol", a fireplace and caludron for boiling water enabling moisture control and chimney for fume exhaust [4].

Jeon Soon, Korean royal family's physician, in his treatise on cooking and crop husbandry called "Sanga Yorok", describes this method and provides a detailed guide for construction of this type of cold frames [4]. The concept of cold frame also spread throughout Europe during the 17th century and different designs were experimentally tested. Today, Netherlands hosts some of the largest cold frames in the world, "some of them so vast that they are able to produce millions of vegetables every year" [3]. Technological and industrial advancements in 1700's improved glass production and construction techniques,

these advancements were also reflected on the cold frames design and construction. A remarkable example of that was the cold frame, then called “orangerie”, at the palace of Versailles. This magnificent structure with a length exceeding 150 meters, width of 13 and height of 14 meters, had a solid roof and its windows were facing the south, letting sun light in for heating the orange trees [2,4].

Later on, orangeries gradually became greenhouses and between 1801 and 1805 in St. Petersburg, a gigantic structure was erected by the order of Czar Alexander-I. It consisted of three buildings, each having a length of 230 meters, that were connected to each other with two additional buildings [2]. The idea of constructing a greenhouse with the house, e.g. in the backyard, became common in England during the 19th century and by the middle of this century, all the necessary techniques required for the successful greenhouse gardening had been developed. Prior to 1870s, in the United States and Europe, the major source of heat for greenhouses was decomposing organic matter (Figure 1.2), however, the lack of control over the amount of generated heat and the shortage of manure supply indicated the need for developing other methods. The substitute method was hydraulic heating system which used water or steam and although its early developments started before 1870 in England, it was the United States which became the center of hydraulic heating systems innovations after 1870 [5].

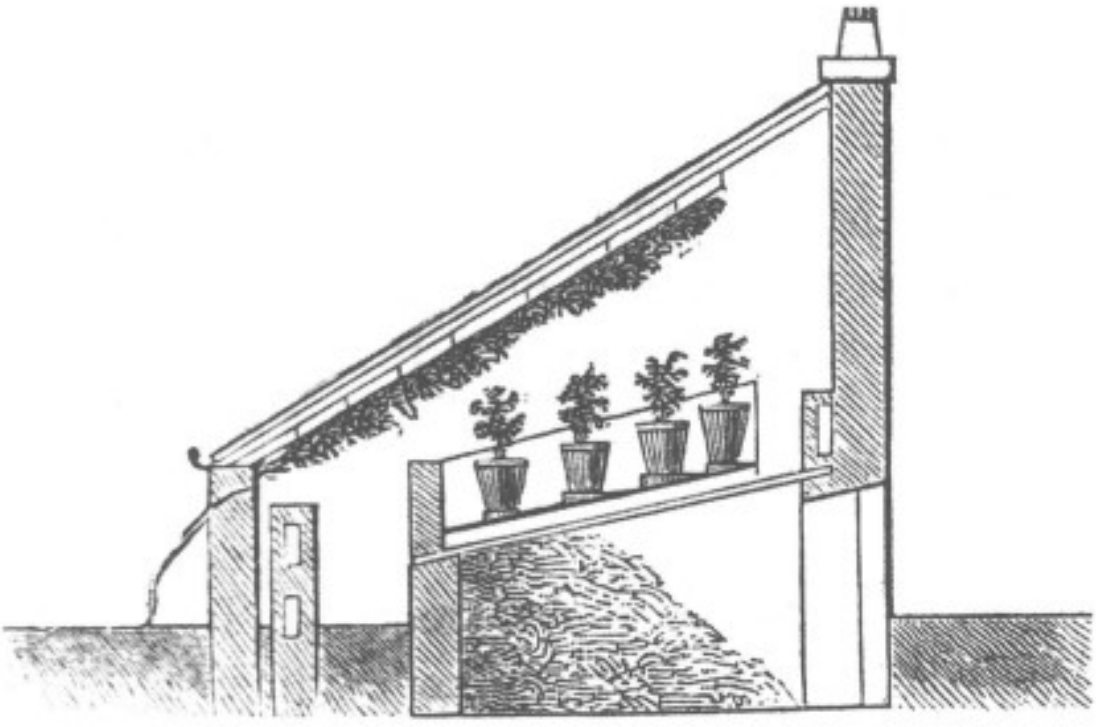

Figure 1.2: Using decomposition of manure to provide the heat in a greenhouse. This method was replaced by hydraulic heating systems after 1870 [5].

Industrial developments improved designs and production techniques, reduced the cost of having greenhouse and made them more available. By the late 1970's, investing one-third the price of a small car would allow one to build a small greenhouse equipped with automatic controls. Since then, a variety of greenhouses have been in use with many of them having a modular design which enables the users to easily expand the structure of greenhouse if needed. Until recent years, the rule of the thumb for greenhouse design and construction was to start with the largest structure that one could afford, but the growing demand for energy conservation has changed that. Nowadays, the recommended approach

is to begin with a smaller modular greenhouse which allows the extension when required [2].

Generally, greenhouse designs fall into two categories: (i) attached to a house, also known as Solarium, and (ii) Freestanding or Greenhouse. The latter comes with some general advantages. Firstly, by placing its long axis in east-west direction, a freestanding design provides every plant in each corner with the maximum light exposure. Secondly, it lets the insect control process be done in a safer and easier manner, since being detached from the residential premises eliminates the risk of exposure to toxic gases for the residents of the premises. Thirdly, freestanding design allows the greenhouse to be used for the purpose of crop drying [2]. Figure 1.3 illustrates the classification of greenhouse systems.

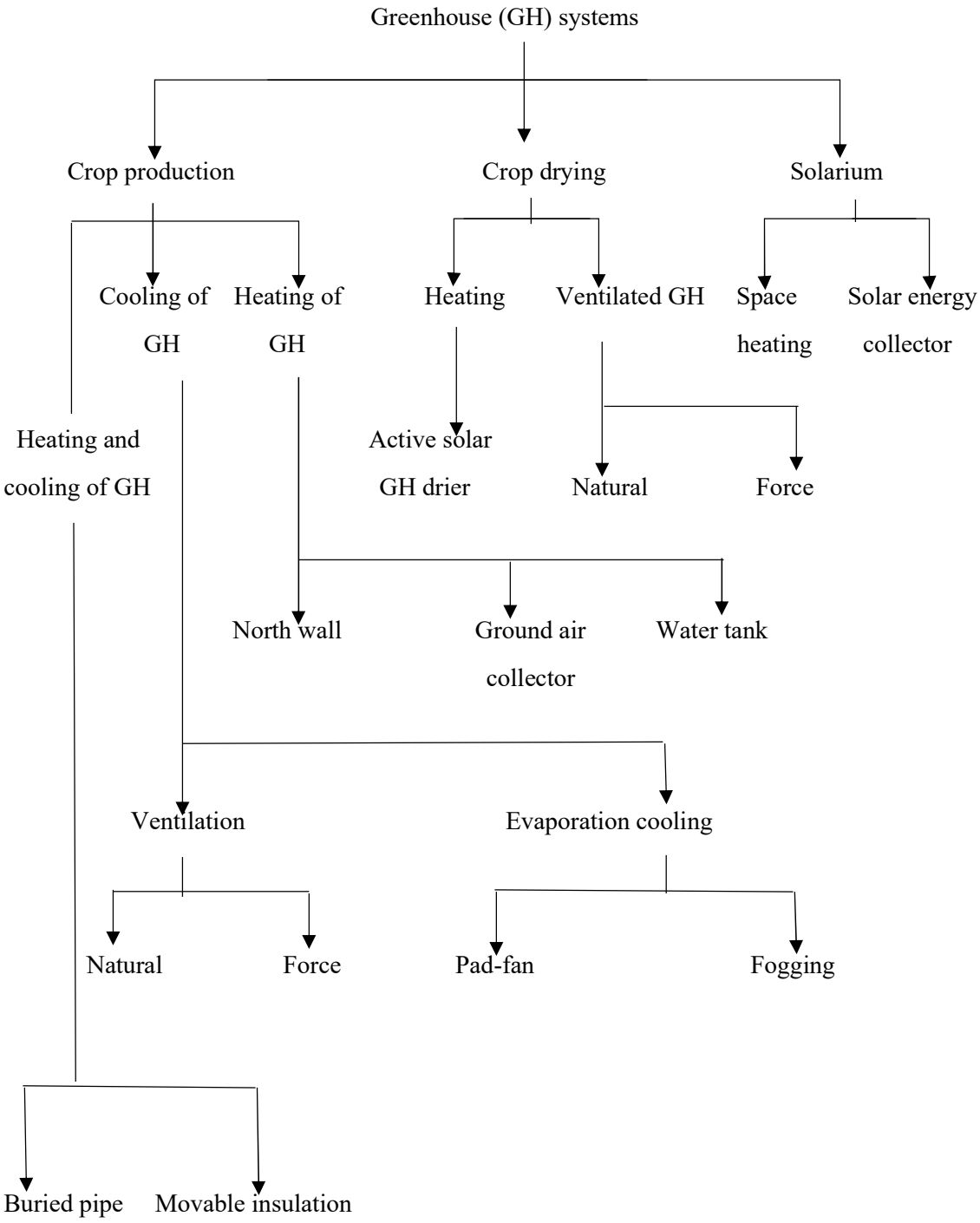

Figure 1.3: Classification of greenhouse systems [2].

1.3 The Need for Four-season Greenhouse

For any plant there is an optimal range of temperature within which they can grow. If the temperature inside the greenhouse exceeds a certain value, the plants can die. Likewise, if plants are exposed to temperatures below a threshold value the plants can also die. In a traditional greenhouse, with no energy management, the plants get exposed to very high and very low temperatures. The latter usually happens on cold wintry nights and the former is likely to occur in daytimes during the summer. The result of this exposure could range from slight damage to the total loss of the plants. One common solution is to equip the greenhouses with cooling and heating systems which would make it possible for them to operate year-round [6]. The downside of using heating and cooling systems, however, is that it would lead to an increase in the total energy consumption, mostly consumed for heating, which subsequently means a decrease in total benefit-to-cost ratio. In order to reduce the need for heating and cooling, people have developed ingenious methods of storing the heat naturally available during the day so that it can be used at night allowing the greenhouse to be functional during all four seasons.

A four-season greenhouse, like traditional ones, is a structure within which the conditions, mainly temperature and humidity, are controlled allowing for the stable growth of plants. The difference, however, is that the design of four-season greenhouses is done with the additional goal of minimizing, if not cutting, the dependence of the structure on the external sources of energy (used to power cooling and heating systems in traditional greenhouses), thus reaching the highest possible level of self-sufficiency and energy efficiency (cost). This goal can be achieved by means of reducing the amount of energy wasted during the

operation of the greenhouse by storing energy readily available (or in excess) during the day to be used during the colder nights. There are two scenarios for heat exchange and they will be discussed in the following: (1) A hot summer day (or any situation where air is at higher temperature than soil), (2) a cold wintry night (or any situation where the soil has higher temperature than air).

When the temperature reaches an upper limit, e.g. during daytime, in a Four-Season Greenhouse, the excessive heat is stored in the greenhouse structure. The storage media varies by design and common choices are: (i) the soil beneath the greenhouse, (ii) a water tank or water pool (with the possibility to be used as fish farming site) in close vicinity or inside the greenhouse. During this process, the direction of energy transfer is from air to the soil and it can happen in two forms. The first form is by convection, and it happens when hot air passes through cold soil. The second form is when vapor content of the humid air loses energy, cools down and eventually condenses into liquid water releasing condensation latent heat which will be absorbed by and stored in the soil. In this process, the temperature of air is regulated by transferring some of air thermal energy to soil and storing it there, instead of just venting the extra energy out of the greenhouse.

When the temperature reaches a lower limit, e.g. during the night, the direction of energy transfer is from soil to air. Circulation of air through the soil forces thermal energy to be transferred from warm soil to colder air. In this process, instead of relying on an external source, the energy that is required to increase the air temperature is supplied by soil.

The last two paragraphs can be summarized as follows: In daytime, air temperature is regulated [cooling] by transferring excess energy to the soil. In nighttime, air temperature

is regulated [heating] by absorbing energy from the soil. This approach not only reduces the total energy consumption, but also improves the quality of production by enabling better management of the key factors that affect the growth of the crops.

1.4 Statement of the Problem

As mentioned in the previous sections, the use of heating and cooling systems increases the total cost of operating a greenhouse. It is reported that the cost of using such systems in traditional greenhouses, predominantly for heating, can cover up to 50% of total operational cost in warmer regions (Southwest United States, Mexico, Spain, etc.) and a hefty 85% in high latitude regions (Canada, Netherlands, England, etc.) [7]. This indicates the need for and the importance of designing and developing solutions which can contribute to the construction of low energy consuming and more energy efficient greenhouses.

1.5 Objectives

The main objective of this work was to attempt to use ANSYS Fluent to model the heat transfer process of four-season greenhouses in an attempt optimize the design of the underground heat storage system. To achieve this goal four types of models were investigated with each of them having their own specific advantages and disadvantages and finally, one of them was selected and tested for different boundary conditions. The details and results will be presented in the following chapters.

1.6 Thesis Outline

Chapter 2 is a literature review of previously published research in the fields of greenhouse design and CFD simulation.

In Chapter 3 an introduction to ANSYS Fluent will be presented. This chapter will include technical details about the software, a theory guide for how the software performs the calculations, different available models which were investigated for our research, as well as instructions and information on how to properly use the software.

Chapter 4 will include the details of our model (geometry design, mesh details, assumptions we made, boundary conditions that were tested, etc.). In this chapter, the results of our simulations will also be presented and comparisons between the results for different boundary conditions will be made.

In Chapter 5, our conclusions will be presented as well as suggestions for the potential future research.

Chapter 2 Literature Review

2.1 Greenhouse Design

In general, components involved in greenhouse design can be divided into four groups: the cladding material, the shape, the orientation, and the climate control systems to manage the microclimate inside the greenhouse (Figure 2.1) [8].

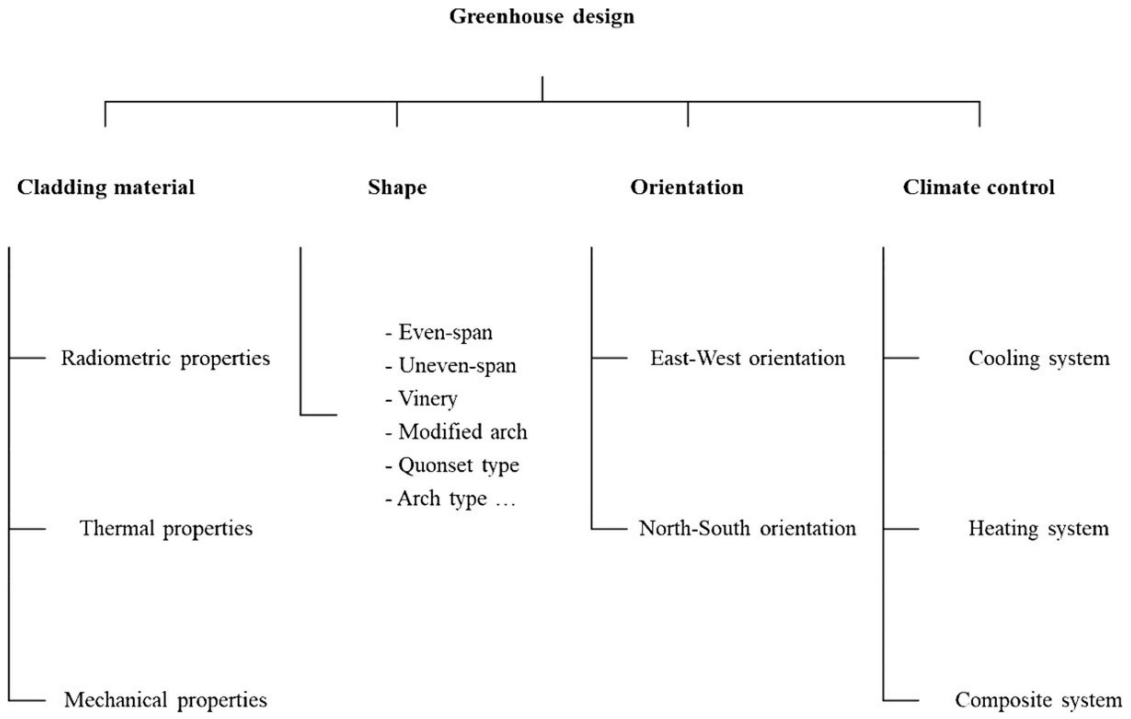

Figure 2.1: Greenhouse design components. Reproduced with permission from [8].

In recent years, various research has been conducted which has led to a better understanding of how each of these four factors plays a role in greenhouse functionality and efficiency [9,10,11,12,15,16]. A selection of these published studies are reviewed in this chapter.

2.2 Covering Material

Traditionally, glass has been the predominant glazing material used in greenhouses all over the world, however, the introduction of plastics as well as the demands to lower the cost of construction have contributed to the wider usage of plastics than glass in recent years. The transition from glass to plastics also forced construction techniques and climate control systems to undergo dramatic changes to adapt to the nature of plastics. Therefore, the common choices for covering material used in greenhouse construction are: single and double glazing, single or double plastic sheets and films or a combination of them. Each of these choices meets certain needs regarding the structural or the functional characteristics of the greenhouse and comes with its own advantages and disadvantages [9].

2.2.1 Radiometric Properties

Solar radiation (illumination) is a free, clean and renewable source of energy, and for greenhouse designers, it is crucial to have a good understanding of how a covering material interacts with solar radiation. When radiation falls upon a material it is either: (1) reflected; (2) absorbed/emitted; or (3) transmitted. Transparent materials allow a large portion of incident radiation to pass through, while opaque materials block the radiation falling upon them. The passage of radiation through a transparent material can be either direct or diffusive. In direct passage, the radiation maintains the same direction while passing through the material with some distortion. On the other hand, when diffusive passage takes place, the material disperses the radiation which causes the rays to deflect in all directions

and form an isotropic distribution. It should be noted that an opaque appearance of a material does not necessarily indicate high or low transmittance. Instead, what is important is the total radiative flux (direct and diffusive). To predict the radiometric properties of a material electromagnetic theory can be applied, however, many assumptions are usually required in the derivations and the effect of surface conditions are generally neglected [10].

Spectral transmissivity τ(λ), of a material is defined as the fraction of perpendicularly incident radiant flux transmitted at a specific wavelength λ, while an average solar transmissivity coefficient τ_s is the average transmissivity over a specific solar waveband, weighted by the wavelength distribution density function in the solar spectrum. This distribution function $P_s(\lambda)$ is the direct normal spectral irradiance at wavelength λ and by integrating $P_s(\lambda)$ over the band $[\lambda_1,\lambda_2]$ the power in the solar spectrum between λ_1 and λ_2 is obtained. The average transmissivity coefficient τ_s of a material to solar radiation can be therefore calculated using:

$$\tau_s = \frac{\int_{\lambda_1}^{\lambda_2} \tau(\lambda) P_s(\lambda) d\lambda}{\int_{\lambda_1}^{\lambda_2} P_s(\lambda) d\lambda} \quad (1)$$

Spectrophotometers can be used to measure the spectral transmissivity τ(λ), while the values for the distribution function $P_s(\lambda)$ as well as for λ_1 and λ_2 can be found in various standards, e.g. E891 and ISO 9050 [10].

The average solar reflectivity coefficient ρ can be defined in the same way as of the average solar transmissivity coefficient τ, while the spectral reflectivity ρ(λ) is measured using

spectrophotometers. Once τ and ρ are determined, the well-known Kirchoff's relationship can be used to calculate the average solar absorption coefficient α [10]:

$$\alpha + \tau + \rho = 1 \quad (2)$$

It should be noted that absorptivity coefficient of a body α can be defined as the ratio of the real emissive power of the body (real radiative power emitted) to the emissive power of a black body at the same temperature. This ratio is also equal to the emissivity coefficient ε of the body. Both these coefficients α and ε may be used to represent the integrated behavior of the greenhouse covering material over all wavelengths [10].

2.2.2 Thermal Properties

The overall thermal behavior (regarding sensible heat transfer) of a covering material is governed by three coefficients, (i) the coefficient of thermal conductivity, (ii) the coefficient of convective heat transfer, and (iii) the overall coefficient of heat transfer, while in applications where vapor condensation takes place, the coefficient of water vapor transfer should also be considered [10].

The coefficient of thermal conductivity *k* of a material is defined as the heat flux density through a unit thickness of an infinite slab of a homogeneous sample of the material in a direction perpendicular to its surface, induced by unit temperature difference at steady-state conditions. This coefficient is calculated as follows:

$$k = QL/A(T_1 - T_2) \quad (3)$$

Where Q is the heat flux through the sample, L is the sample thickness, A is the area of the sample, and ($T_1 - T_2$) is the temperature difference between the hot and cold sides of the sample [10].

The coefficient of convective heat transfer h for a covering material is defined as the heat flux of the covering to its surroundings, induced by the unit temperature difference between the covering and the air at a location far away from the covering. This coefficient is represented with the subscripts h and c for hot and cold surfaces respectively and is calculated as follows:

$$h_h = Q/A(T_h\text{-}T_1) \tag{4}$$

$$h_c = Q/A(T_2\text{-}T_c) \tag{5}$$

The overall coefficient of heat transfer K (or K value) is assigned to composite materials and accounts for the overall heat transfer through the material due to conduction and convection. It is calculated as follows:

$$K = \frac{1}{\frac{1}{h_h} + \frac{1}{h_c} + \sum_j \frac{d_j}{k_j}} \tag{6}$$

Where h_h and h_c are the coefficients of convective heat transfer for the inner (usually hotter), and for the outer (usually colder) sides of the material, respectively, d_j represents the thickness of the j^{th} element constituting the material, and k_j is the coefficient of thermal conductivity of the material composing the element. It should be mentioned that Equation (6) does not take neither thermal radiation exchange nor condensation into account,

therefore it is generally expected that the calculated value of the coefficient *K* would be lower than the real value. An alternative equation which returns more practical values than equation (6), consists of calculating *K* when *Q,* the heat flux density through the material separating two enclosures with air temperatures T_h and T_c ($T_h > T_c$), is known [10]:

$$K = Q/A(T_h\text{-}T_c) \quad (7)$$

Thermal and radiometric properties of greenhouse covering materials can sometimes be related to each other. For instance, using composite materials, such as double-glazing sheets or coated glass with low emissivity, generally provide higher insulation values which means better energy conservation. The drawback, however, is the reduction of the light transmittance. For example, the interception of diffuse light by a double-glazing system leads to around 10% light loss compared to a single-glazing system. According to experimental data, "1% light loss is equal to 1% production loss" [9], so double-glazing systems are no longer in use as greenhouse roofing and double-web plastic sheets are utilized only on a small scale. As alternatives, single and double thermal movable screens are used for insulation.

2.2.3 Mechanical Properties

The design of greenhouse structures follows the same standard procedures applied to the corresponding conventional types of structures. In general, steps on greenhouse design are taken according to the corresponding standards for common civil structures, however, there are some needs and requirements regarding the greenhouse design which are unique to this

area and thus must be met independently. This particularity in greenhouse design has led to special standards specific to greenhouse design being issued at the national level by some countries. There have been reports of efforts being made to prepare European standards for the design of greenhouse structures [9].

There are four general sub-categories which may be grouped under the umbrella term "Mechanical Properties": (1) loading conditions, (2) structural design, (3) installation, and (4) environmental effects [9].

2.2.3.1 Loading Conditions

There are various factors that can cause loading and should be considered when calculating actions for greenhouses, but the most important ones are: snow and wind loading, loads due to hail, loads due to supporting plants and equipment, service loads, and combinations of these. The loading conditions in a greenhouse can be related to the behavior and design of coverings in two ways: directly and indirectly. Directly related means the covering material acts as a load carrying component in the greenhouse structure and directly bears the loadings. Therefore, the load due to hail may be related to the impact resistance of covering material, the snow and wind loading may be related to bending, shear/tear and tensile properties and likely to the dynamic behavior of the material. Indirectly related means the covering material acts as an intermediary component transferring loads to the structural framework through the development of load carrying and redistribution mechanisms. When the loading is indirectly related to the covering, it may be significantly affected by the details of the covering materials installation [9].

2.2.3.2 Structural Design

The most important role of the greenhouse and its covering is to provide protection for the plants and crops against the harsh climate conditions (extreme temperatures, strong wind, snow, etc.) and natural threats (pests and infections). In general, and specifically in areas where natural light levels are normally low, it is crucial to design and implement greenhouses which allow maximum light intensity inside. Therefore, designers aim to employ as less structural parts as possible, since a higher number of parts generally means more light blocking area and more shadows inside the structure. In other words, to reach the highest possible light transmittance, the covering materials should have the largest possible unsupported area. At the same time, the structural parts and the whole greenhouse structure must be strong enough to bear different loads (from snow, hail, rain, wind, the weight of structure itself, etc.) to provide reasonable margins of safety. So, it appears that the requirements for the maximum light transmittance counteract the requirements of safety and structural stability. Thus, the ideal design of a greenhouse should contain a balance among:

(1) The collective structural design and the properties of individual structural components.
(2) The specific physical and mechanical properties which dictate the functional and structural behavior of cladding materials.
(3) The crops requirements regarding the light intensity and temperature inside the greenhouse structure [9].

2.2.3.3 Installation

One of the key factors which affects the overall mechanical performance of the covering is the installation of the covering material to the greenhouse structure. Therefore, it is important to carefully consider the details of installation when evaluating the mechanical properties of the covering materials. Three widely used covering materials are glass, semi-rigid plastics and plastic films [9].

Although usually referred to as fragile, glass is a strong material if used properly and loaded in the correct way. Limiting the chances of breakage of glass coverings requires design rules to be applied to the structures supporting the glass panels. Such rules, in general, aim to limit the deformation in structural components providing support to the glass panels. Some of such rules are as follows:

The maximum bending deflection (u) of the gutters, purlins in the roof and ridge profiles is given by: $u \leq L/(650\text{-}100n) \leq L/250 \leq 18$ *mm,* where L is the distance between the rafters/trusses and n is the number of panels within this distance.

The maximum bending deflection (u) of the gable supporting parts is given by: $u \leq L/150 \leq 25$ mm, where L is the length of gable column or gable purlin.

The maximum bending deflection (u) of glazing bars for the support of rigid materials is given by: $u \leq L/100 \leq 20$ mm, where L is the span of the glazing bar [9].

In addition to glass, semi-rigid plastics and plastic films are widely used as coverings in greenhouse design and construction. Same as glass panels, there are standard rules limiting the deformation of structural components which provide support for semi-rigid sheets.

According to this standard, the supporting width for plastic sheets should take into account some properties of the sheet material including: bending limitations, thermal expansion and shrinkage as well as greenhouse circumstances. For example, in France, depending on the material and the structure, the assembly of semi-rigid sheets on the roof is specific and does not follow the same guidelines. In Germany, however, no specific guideline applies on the installation of plastic covering materials to the greenhouses structure [9].

The third group of covering material used in greenhouse construction is plastic films. In general, film coverings are secured to the structure using aluminum or plastic clamps or clips which fit in an open hollow profile (Figure 2.2 (a)). Potential problems for such fittings would be the strength of the clips and clamps themselves or the possibility of the male part coming out of the socket (unlocking the clamp). Some clips have sharp edges which can tear the plastic films. There are also more expensive specially designed clamp fittings which provide more strength and require the film to be welded all along the sides (Figure 2.2 (b)). In non-standardized timber greenhouses such as grower-built ones in Greece, (and likely other places as well), slats are nailed along with the film onto the wooden structural elements. In such cases, tearing failures frequently happen either at the locations where the film is initially pierced or due to tension caused by wind loading [9].

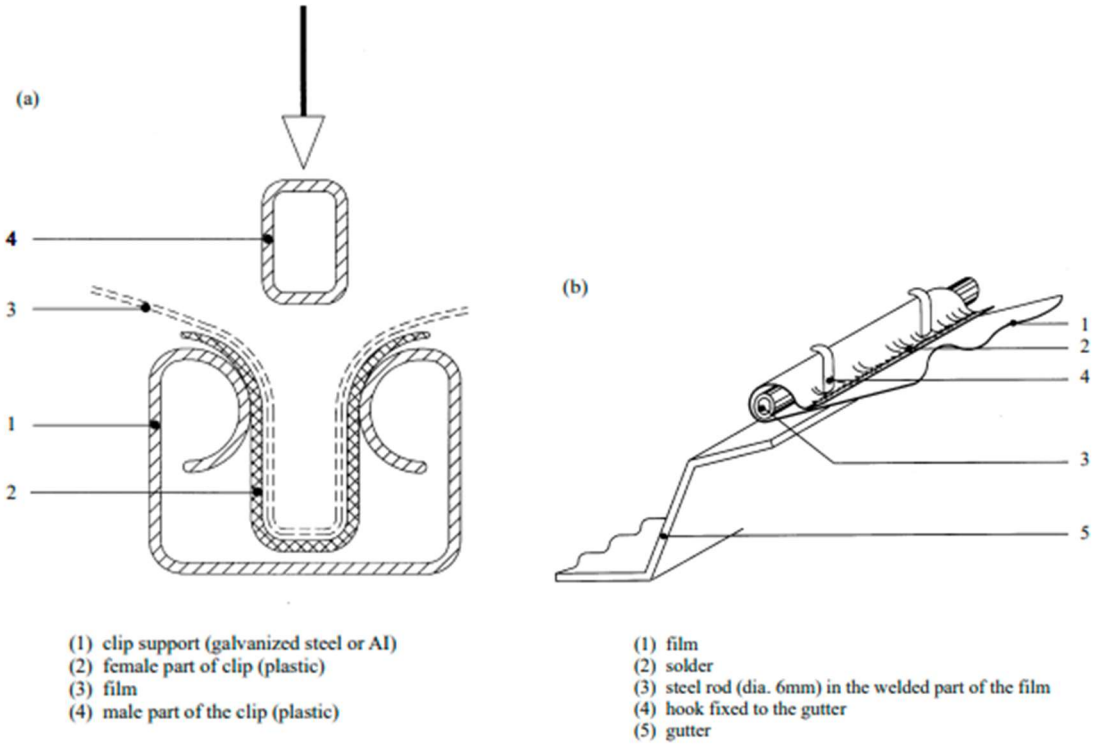

Figure 2.2: Illustration of clamps used for the purpose of securing the plastic films to the greenhouse structural parts; a) simple clip b) welded film. Acquired with permission from [9].

2.2.3.4 Environmental Effects

Environmental effects on the properties of the greenhouse covering materials can vary from negligible to severe, these effects depend on the material itself, properties under consideration, and the existing environmental factors. Regarding the glass coverings, the main challenge is that glass will break rather than deform under strong impact and although it is capable of surviving strong compressions, it is relatively weak under tensile stress. Ageing of glass is generally considered to be negligible, however, greenhouse practice suggests that glass may become more fragile after 15 years of life. The usage of glass also comes with a loss of light transmission as the dirt accumulates on its surface and it is not

an easy task to clean the glass, except through the use of chemicals which, especially in greenhouse environments, can be potentially problematic for the plants inside [9]. The mechanical and physical properties of most semi-rigid plastic sheets decay under environmental conditions. The degree of deterioration varies in different cases, for example, polyesters and PVC suffer from UV radiation, while acrylics are mainly affected by chemicals. In most cases, the loss of light transmittance due to natural ageing is negligible as compared to the loss of strength, although PVC may reveal 20% transmittance loss over 10 years [9]. The guarantee offered in the market for plastic films with thickness ranging from 120 μm to 200 μm generally covers 2 to 3 years. Mechanical and physical properties of plastic films change over time and affect the durability of the films. For example, UV ageing leads to the reduction of the elongation of the material at the breaking point. Other problems are related to light transmittance. Developments of UV stabilized films helped in dealing with UV ageing, but new challenges emerged. For instance, Sulphur and Chloride, active substances in chemicals used in greenhouses, block the effect of HALS (Hindered Amide Light Stabilizers), which are used as UV stabilizing substances for PE films. Ni salt, another stylizing substance, is not affected by Sulphur and Chloride. The effects of stabilizing substances on the recycling potential of plastics as well as other environmental impact implications have recently emerged as major considerations [9].

2.3 Shape

Among all types of single span greenhouses, the five most frequently used are: even-span, uneven-span, vinery, Quonset and modified arch (Figure 2.3).

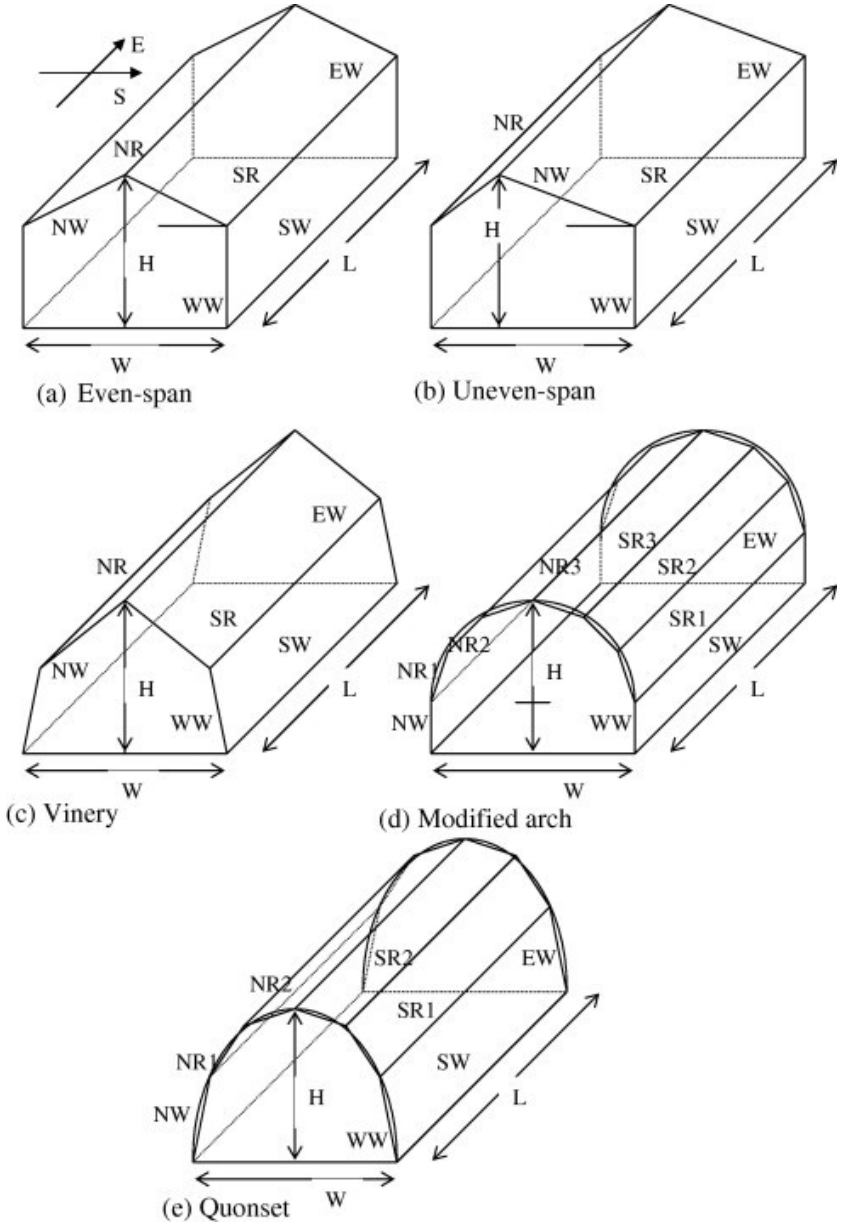

Figure 2.3: Five most frequently used shapes of greenhouses. Acquired with permission from [11].

A study comparing these five shapes was done where a mathematical model was used for computing transmitted total solar radiation. The results of that study were then used in a transient thermal model for computing hourly inside air temperature. The computational results predicted that, keeping main geometrical characteristics such as length, width and height the same, the uneven-span shape, at all latitudes and during each month of the year, will have the best performance in terms of maximizing the solar radiation absorption, while the Quonset type will collect the least solar radiation. The results also indicated that the temperature of air inside will be affected by the shape of the greenhouse, and maximum and minimum values will be registered for uneven-span and Quonset types respectively. These results were experimentally validated for an uneven-span shape during a typical day in summer at Ludhiana, Punjab, India (31°N and 77°E) [11]. In another study, the performances of the five aforementioned greenhouse shapes with the addition of arch type were compared. According to the results of this study, the single span greenhouse oriented East-West, compared to other shapes, receives around 8% more solar radiation during each month of the year. The experimental validation of these results was conducted in a single-span greenhouse in the North-West of Iran and a good agreement between predicted and measured values was obtained [12]. A study was done using a mathematical model to investigate the effects of greenhouse design on energy conservation and the results showed that, under cold climatic conditions of northern India, an arch type requires 4.2% and 2.6% less heating demand as compared to Quonset and gable shapes [13]. In another study concerning the heating demand for cold climates in India, it was found that the uneven-span shape greenhouse is the most suitable from a heating point of view [14].

Regarding the multi span greenhouses, it has been shown that the ventilation rate is significantly affected by the number of spans [8] and it has been confirmed that there is a decay relationship between the number of spans and the ventilation rate [15,16].

2.4 Orientation

Due to the dynamic change of solar trajectory and solar radiation intensity at different latitudes, it is crucial to determine the suitable greenhouse orientation [17]. Computational results as well as experimental validation showed that, at all latitudes except near the equator, East-West orientation is favorable for year-round greenhouses, since the total radiation received by the greenhouse, constructed in East-West orientation, is greater in winter and lesser in the summer [11,18]. The impact of greenhouse orientation in the Mediterranean zone was investigated in a study and the results indicated that, for crops at early stages of growth, East-West orientation was not suitable. On the contrary, North-South orientation was favorable due to its contribution to the homogeneity of microclimatic conditions in greenhouse leading to better yield [19].

2.5 Climate Control

To determine the optimal operating conditions for greenhouses, it is necessary to study and understand how different parameters influence the heating/cooling demand inside the

greenhouse. Thermal modeling as well as mathematical simulation tools have been used for this purpose [8].

2.5.1 Mathematical Modeling

Mathematical modeling, in general, refers to the process of formulating an abstract problem in terms of a mathematical language to describe the complex behavior of a real system. Mathematical models are quantitative models usually expressed in terms of ordinary and/or partial differential equations. Mathematical modeling is widely employed by researchers in the fields of natural sciences, computing, engineering, meteorology, economics, and finance [39]. Several studies have been conducted by employing one-dimensional models and dividing the greenhouse into multiple zones in an attempt to accurately predict the thermal behavior of each zone [8]. A study was done by dividing the greenhouse into four horizontal zones and using a dynamic model to determine the air temperature in different zones. According to numerical analysis, the authors concluded that the plant temperature is more affected by the heat capacity of the plant and the relative humidity than by the air temperature with the temperature differences between the different zones of the greenhouse being negligible. The experimental validation of the results was done for a typical winter day of the month of December and a fair agreement between measured and calculated data was obtained [20]. Evaporation is also an important factor involved in determining the thermal behavior of the greenhouse and it has been considered in several models. A transient model was suggested by Cooper and Fuller [21] for

simulating the interaction between the crop, environment, and greenhouse structure to predict the crop yield and energy consumption. In their model, a number of separate units interacting with each other constitute the greenhouse and to simulate dehumidification and cooling processes, an enthalpy wheel and an evaporative cooler are included respectively. Greenhouses have also been studied as solar energy collector units. A thermal model developed by Boulard and Baille [22] examines the performance of greenhouse using a single energy balance equation where two main parameters are overall heat loss coefficient and solar efficiency factor. According to the authors, their model, despite being very simplified, explains around 80% of the variability of the collected solar energy in a greenhouse. A study was conducted with the purpose of investigating the impact of the construction parameters of greenhouses on solar energy collection efficiency under western European climate [23]. The transmittance of the greenhouse frame, radiometric properties of the covering and floor, and the type of condensation (as film or as drops) were three parameters investigated in this study. The results showed that the greenhouses absorb about 66% of available solar radiation, which is considered poor efficiency and is due to the fact that greenhouses are fixed structures. The results also pointed out that most of the solar energy entering the greenhouse is consumed by vegetation.

2.5.2 Computational Fluid Dynamics

Although there are difficulties in modeling turbulent transfers, simulations using CFD software are becoming more realistic and able to offer a good level of accuracy in

describing the main features of the distributed climate inside the greenhouse [24]. A 2D transient CFD model demonstrated the possibility of growing plants, without significant drop in yield, with as much as 20% less water consumption by examining different irrigation profiles [25]. Studying the cooling of a solar greenhouse using CFD software showed that, in a solar greenhouse equipped with removable back walls, the average and the highest registered air temperatures are reduced by 1.7 °C and 5.8 °C respectively, as compared to a traditional greenhouse with a brick back wall [26]. Radiation models have also been added into CFD models to account for convective and radiative energy exchange between the floor and the covering of a greenhouse, instead of the conventional coupling approach based on energy balance [27]. The condensation inside the greenhouse has also been simulated and studied using CFD [28]. The results pointed out that the roof has the lowest temperature and thus is a heat sink for the water vapor produced inside the greenhouse. The heat transfer losses by radiation, especially for soils with low heat flux values, were also observed. A comparison of three different turbulence models (k-ε Standard, k-ε RNG and k-ε Realizable) in ANSYS Fluent for an empty tunnel type greenhouse in France, showed that, for this arrangement, the k-ε Standard model offers the most accuracy [29]. Regarding the similarities and differences among these three models, it can be mentioned that the simplest of the "complete models" of turbulence are the two-equation models. The “k-ε Standard” model in ANSYS Fluent which was proposed by Launder and Spalding falls within this class of models. The “k-ε Standard” model is a semi-empirical model is based on the model transport equations for the turbulence kinetic energy ($\boldsymbol{k}$) (equation 8) and its dissipation rate ($\boldsymbol{\varepsilon}$) (equation 9). The model transport equation (equation 8) for $\boldsymbol{k}$ is derived from the exact equation, while the model transport equation

for $\boldsymbol{\varepsilon}$ was obtained using physical reasoning and bears little resemblance to its mathematically exact counterpart. The assumption made in the derivation of this model is that the flow is fully turbulent, and the effects of molecular viscosity are negligible [33]. The “k-ε RNG” model was derived using a rigorous statistical technique (renormalization group theory). It is similar in form to the “k-ε Standard” model, but also has some refinements: The RNG model has an additional term in its dissipation rate ($\boldsymbol{\varepsilon}$) equation which significantly improves the accuracy for rapidly strained flows. The effect of swirl on turbulence is included in the RNG model, enhancing accuracy for swirling flows. The RNG theory provides an analytical formula for turbulent Prandtl numbers, while the “k-ε Standard” model uses user-specified, constant values. While the “k-ε Standard” model is a high-Reynolds-number model, the RNG theory provides an analytically-derived differential formula for effective viscosity that accounts for low-Reynolds-number effects. Effective use of this feature does, however, depend on an appropriate treatment of the near-wall region. These features make the “k-ε RNG” model more accurate and reliable for a wider class of flows than the “k-ε Standard” model [33]. The “k-ε Realizable” model is a relatively recent development and differs from the standard “k-ε Standard” model in two important ways: The realizable “k-ε Realizable” model contains a new formulation for the turbulent viscosity. A new transport equation for the dissipation rate ($\boldsymbol{\varepsilon}$), has been derived from an exact equation for the transport of the mean-square vorticity fluctuation. The term "realizable" means that the model satisfies certain mathematical constraints on the Reynolds stresses, consistent with the physics of turbulent flows. Neither the “k-ε Standard” nor the “k-ε RNG” models are realizable [33]. A more comprehensive

description of these three models theories and their applications to turbulence can be found in ANSYS Fluent Theory Guide [33].

$$\frac{\partial}{\partial t}(\rho k) + \frac{\partial}{\partial x_i}(\rho k u_i) = \frac{\partial}{\partial x_i}[\left(\mu + \frac{\mu_t}{\sigma_k}\right)\frac{\delta k}{\delta x_j} + G_k + G_b - \rho\varepsilon - Y_m + S_k \tag{8}$$

$$\frac{\partial}{\partial t}(\rho\varepsilon) + \frac{\partial}{\partial x_i}(\rho\varepsilon u_i) = \frac{\partial}{\partial x_i}[\left(\mu + \frac{\mu_t}{\sigma_\varepsilon}\right)\frac{\delta\varepsilon}{\delta x_j} + C_{1\varepsilon}\frac{\varepsilon}{k} + (G_k + C_{3\varepsilon}G_b) - C_{2\varepsilon}\rho\frac{\varepsilon^2}{k} + S_\varepsilon \tag{9}$$

In above equations, u_i is the velocity component in corresponding direction, μ_t is turbulent (or eddy) viscosity, σ_k and σ_ε are the turbulent Prandtl numbers for k and ε, respectively, G_k represents the generation of turbulence kinetic energy due to the mean velocity gradients, G_b is the generation of turbulence kinetic energy due to buoyancy, Y_m represents the contribution of the fluctuating dilatation in compressible turbulence to the overall dissipation rate, S_k and S_ε are user-defined source terms, and $C_{1\varepsilon}$, $C_{2\varepsilon}$ and $C_{3\varepsilon}$ are constants as follows:

$$C_{1\varepsilon}=1.44,\ C_{2\varepsilon}=1.92,\ C_{3\varepsilon}=0.09,\ \sigma_k=1.0,\ \sigma_\varepsilon=1.3$$

As it was discussed, there are several factors involved in the overall performance of greenhouses. Some of these factors are related to the physical properties of the materials used in greenhouse construction (e.g. covering materials) and how these materials interact with the external factors such as solar radiation. Some other factors, on the other hand, concern the processes which take place inside the greenhouse structure and how the internal

greenhouse environment (air, moisture, soil) works as an isolated microclimate. There have been various attempts to model and study these factors and gain a better understanding of greenhouse microclimate [25,27,28,29]. Computer assisted modeling, especially in recent years, has attracted the attention of many researchers who contributed to numerous advancements in the field, however, due to multi-component and complex nature of the field, there remains great potential for further work. CFD simulation softwares have proven to be powerful tools with great capabilities to be utilized in the field of greenhouse research. Energy consummation and conservation are very important factors in both domestic and industrial greenhouse designs, since it can contribute to making greenhouses more energy efficient, increase yield, and lead to the greater benefit-to-cost ratio. It is therefore concluded that developing new methods and modeling different scenarios in which energy consummation and conservation is studied is necessary and CFD tools can be employed for this purpose.

Chapter 3 An Introduction to ANSYS Fluent

3.1 Definition of CFD

CFD is an abbreviated term which stands for Computational Fluid Dynamics is a field which focuses on model studies of fluid behavior. The governing equations for a fluid can be obtained by applying three conservation laws of classical mechanics (conservations of mass, momentum, and total energy) to the fluid. The results will be a set of (e.g. for a fluid in 3 dimensions it is described by five equations related to mass, energy and three momentums) coupled, non-linear partial differential equations, which for most engineering problems, are impossible to be solved analytically. Despite that, obtaining approximate computer-assisted solutions to answer a variety of needs in many physical problems is achievable and that is the main objective of CFD algorithms [30].

3.2 CFD Code Structure

CFD codes are written based on numerical algorithms which can handle fluid flow problems. To provide better accessibility and ease of use, all commercial CFD packages feature user interfaces which enable the user to input the problem parameters and inspect the results. The three main constituents of a CFD code are: the pre-processor, the solver, and the post-processor [31]. These three components are briefly discussed in the next three sections.

3.2.1 Pre-processor

In the pre-processing stage, the inputs of the flow problem are fed into the CFD code through a user interface, where they will be interpreted to become readable by the solver. Typical activities done by the user at this stage are:

- Designing and defining the geometry of the "Computational Domain" or the "Region of Interest".
- Generating the grid (mesh); dividing the domain into several smaller sub-domains (cells) which do not overlap.
- Selecting the physical and/or chemical phenomena that the user wishes to model.
- Defining the properties of the fluid(s) (and the solid(s) if appropriate).
- Specifying the proper boundary conditions.

The solution of a flow problem, which includes pressure, temperature, velocity, density and turbulence, is determined at nodes inside each cell. In general, the accuracy of a CFD solution will improve as the number of cells in the mesh goes up, however, higher mesh count means more computational cost. Thus, it is important to achieve the optimal state in meshing, where the number of cells in the mesh is neither too little to make the solution inaccurate nor too high to demand more than enough computational resources. Optimal meshes usually are not uniform, meaning that they are finer in regions where high variation in flow properties are expected to happen (areas where large gradients occur such as elbows and near wall regions) and coarser in areas where fewer changes are expected to occur [31].

3.2.2 Solver

Numerical solution techniques can be divided into three main branches: spectral methods, finite element, and finite difference. In the spectral methods, the solution is approximated as an expansion in terms of the spectral basis functions (which are infinitely differentiable global functions) and the selection of coefficients in the expansion that satisfies the differential equation the best is then sought [36]. In the finite element method, the domain is divided into a set of simple subdomains called finite elements. This step is called discretization of the domain. The next step involves seeking continuous, often polynomial, approximations of the solution over each element. In the final step, solutions of different elements are assembled by imposing interelement continuity of the solution and the balance of interelement forces [37]. In finite difference method, the same as the finite volume method, the first step is the discretization of the domain. Next, the derivatives in the governing differential equations are approximated by using the truncated Taylor series expansions [36]. A comprehensive comparison among the three models can be found in [38] and a summary of this comparison is represented in table 3.1.

Table 3.1: Comparison of spectral, finite element and, finite difference methods [38].

Method / Attribute	Spectral	Finite element	Finite difference
Trial Solution	Global	Local	Local
Ease of Coding	Fair	Good	Very good
Flexibility	Fair	Very good	Good
Accuracy per unknown	Very good	Good	Fair
Computational efficiency	Very good	Good	Good
Main strength(s)	High accuracy	Flexibility	Economy
Main weakness	Inflexibility	Economy	Ease of coding

Since most widely used CFD codes are developed based on the finite difference approach, we will focus on the finite volume method, a special finite difference formulation. A numerical algorithm works according to three main steps:

- First, the governing equations of the fluid flow are integrated over all cells of the computational domain. This step is called the “Control Volume Integration”.
- Second, integral equations are then converted into a set of algebraic equations. This step is referred to as “Discretization”.
- Finally, iterative methods are used to solve the algebraic equations.

The control volume integration separates the finite volume method from the rest of the CFD approaches. The outputs of this step contain the conservation of relevant properties for each finite size cell. One of the main reasons that makes finite volume method favorable among researchers, as compared to other techniques, is that in this method the relationship between the numerical algorithm and the underlying conservation principles can be easily perceived and simply understood. Consider a general field variable of the flow φ, e.g. a momentum component or energy, the conservation of this variable within a finite volume can be shown as an equilibrium between different processes contributing to increasing or decreasing it. This equilibrium can also be expressed as below:

$$\begin{bmatrix}\text{Rate of change of } \varphi \text{ in the control volume with respect to time}\end{bmatrix} = \begin{bmatrix}\text{Net rate of increase of } \varphi \text{ due to convection into the control volume}\end{bmatrix} + \begin{bmatrix}\text{Net rate of increase of } \varphi \text{ due to diffusion into the control volume}\end{bmatrix} + \begin{bmatrix}\text{Net rate of creation of } \varphi \text{ inside the control volume}\end{bmatrix}$$

CFD codes are equipped with the discretization techniques to tackle the key transport phenomena, convection (transport due to fluid flow), and diffusion (transport due to variations of φ by spatial position). The source terms (related to the creation or termination of φ) and the rate of transformation of φ by time are also taken care of using these techniques. Since the underlying physical phenomena are complex and non-linear by nature, iterative methods are required to obtain the solution. The most commonly used methods are: TDMA (Tri-Diagonal Matrix Algorithm) line-by-line solver of the algebraic equations, and the SIMPLE (Semi-Implicit Method for Pressure Linked Equations) algorithm to ensure pressure and velocity are properly linked. Commercial codes may also

feature more recent methods such as Gauss-Seidel point iterative, which comes with conjugate gradient methods and multigrid accelerators [31].

3.2.3 Post-processor

Same as pre-processing, the post-processing field has recently benefited from a huge number of advancements. Nowadays, the leading CFD packages offer multi-purpose data visualization tools. These tools enable the user to execute various actions including:

- Displaying the geometry and grid
- Plotting vectors
- Plotting different contours
- Plotting 2D and 3D surfaces
- Tracking particles
- Manipulating the viewing (translation, rotation, scaling, etc.)
- Generating color postscripts

More recent advancements also include turning dynamic results into animations as well as the ability to export data into other codes for further processing. The graphical capabilities of CFD codes in post-processing and output exportation, as in many other branches of "Computer Assisted Engineering", have dramatically impacted the communication of ideas even to non-specialists [31].

3.3 ANSYS Fluent

ANSYS is a powerful Multiphysics simulation software developed and marketed by the American multinational company ANSYS, Inc. The software contains many modules (systems) such as Fluent, CFX, Mechanical, Thermal, etc. with each of them designed and developed to answer certain needs. In this chapter the focus is on the Fluent module.

3.3.1 Getting started

The ANSYS workbench contains several boxes and extensions such as Toolbox, Project Schematic box, Messages box, etc. (Figure 3.1).

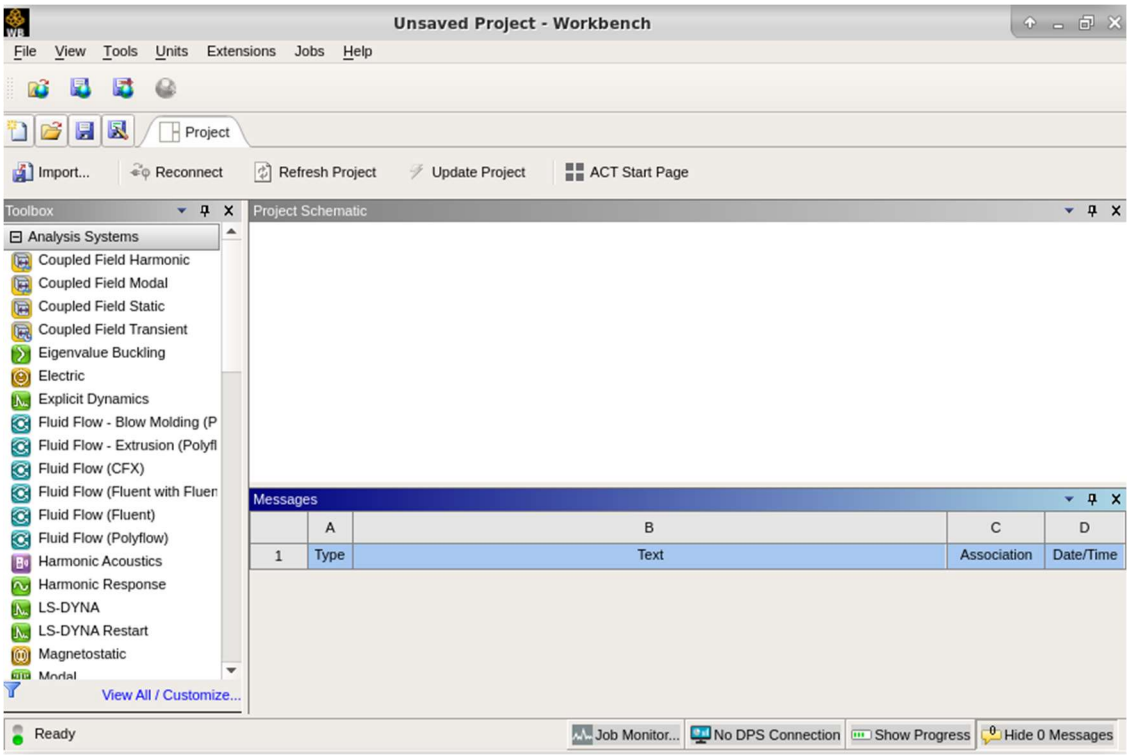

Figure 3.1: A view of ANSYS workbench.

To start a Fluent project, the user needs to click on “Fluid Flow (Fluent)”, located under “Analysis Systems” in the Toolbox, hold and then drag it into the Project Schematic box. Any Fluent project consists of five components: Geometry, Mesh, Setup, Solution, and Results (Figure 3.2). It is also possible to access each of these components individually and after completing each step, the user can then transmit the generated data into the next component (for example, designing the geometry and transmitting the data into the Meshing step), save it for later use, or export it to be used in external applications. Geometry, Mesh, and most of what is done in the Setup step are parts of the pre-processing part in a CFD project. The last step during the setup part is to start the Solver. Solution and Results steps are considered as post-processing.

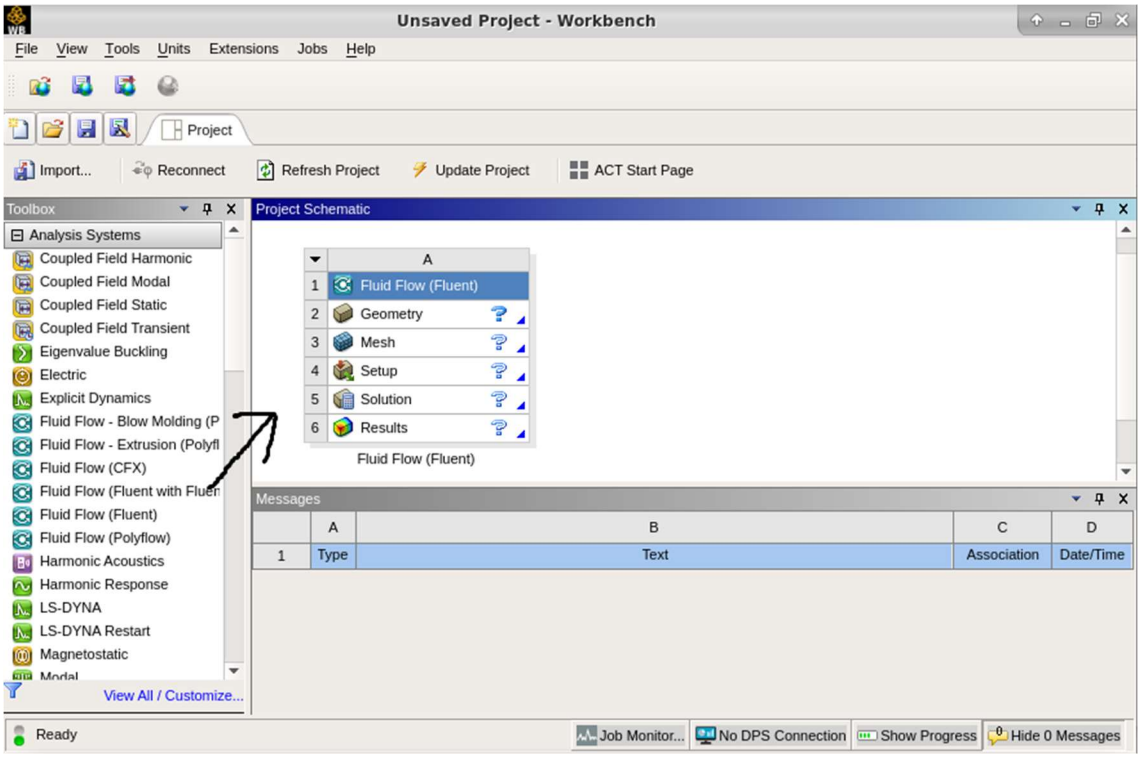

Figure 3.2: A typical Fluent project consists of five components: Geometry, Mesh, Setup, Solution and Results, which must be completed in order.

3.3.2 Geometry

The first step of a Fluent project is to define the Computational Domain, which is done by designing the geometry or the area of interest in 2D or 3D space. By right clicking on the "Geometry" tab, the user can either choose from one of the available designing software (DesignModeler and SpaceClaim) or import a geometry from an external application. All of this work has been done using the DesignModeler application. DesignModeler is a powerful tool used for defining and designing 2D and 3D geometries for a Fluent project and other simulation software. It features various options of which some of them are outlined in the followings with brief description for each option:

- In addition to basic planes (XY, YZ, ZX), users can also define their desired plane as required by the project specifications.
- Under the "Create" tab, by choosing "primitives", the user can select from basic geometrical elements such as cube, sphere, box, cylinder, cone, etc. and then proceed to set other properties of the selected shape (coordinates of the center and/or edges, the length of X, Y and Z components, the radius, etc.). The "Boolean" option is another useful feature which allows the user to unite or subtract two or more geometrical shapes from each other.
- It is also possible to generate desired shapes from scratch. For instance, by drawing a rectangle and a line, and then using the "Revolve" option under the "Create" tab, the user can generate an entire cylindrical shape (360° rotation) or a fraction thereof (less than 360° rotation). Using the "Thin/Surface" option also allows the user to define the inner and outer thickness for a cylindrical shape.

- Under the “Concept” tab, options such as “Lines From Points” and “Surfaces From Edges/Faces” (for 2D applications) are accessible.
- The “Tools” tab contains some practical features including: “Freeze”, used when the user wishes to prevent two or more conjugate geometries from merging and sharing a mesh. The opposite action can be executed using the “Merge” option. The “Fill” option can also be useful in many designs, for example when designing a pipe through which a fluid is flowing.
- Units of the geometry can be selected and altered under “Units” tab.
- At the end of designing the geometry, there are cases where two or more domains exist, e.g. the pipe and the fluid inside it. Although these are considered separate “bodies”, one solid and one fluid, to have a conformal mesh in the meshing part they still need to form a single “part”. This can be done by selecting both bodies and then clicking on ”Form New Part” option, which ensures the generation of a conformal mesh in the next step.

Figure 3.3 illustrates the view of a DesignModeler project showing a simple cylinder.

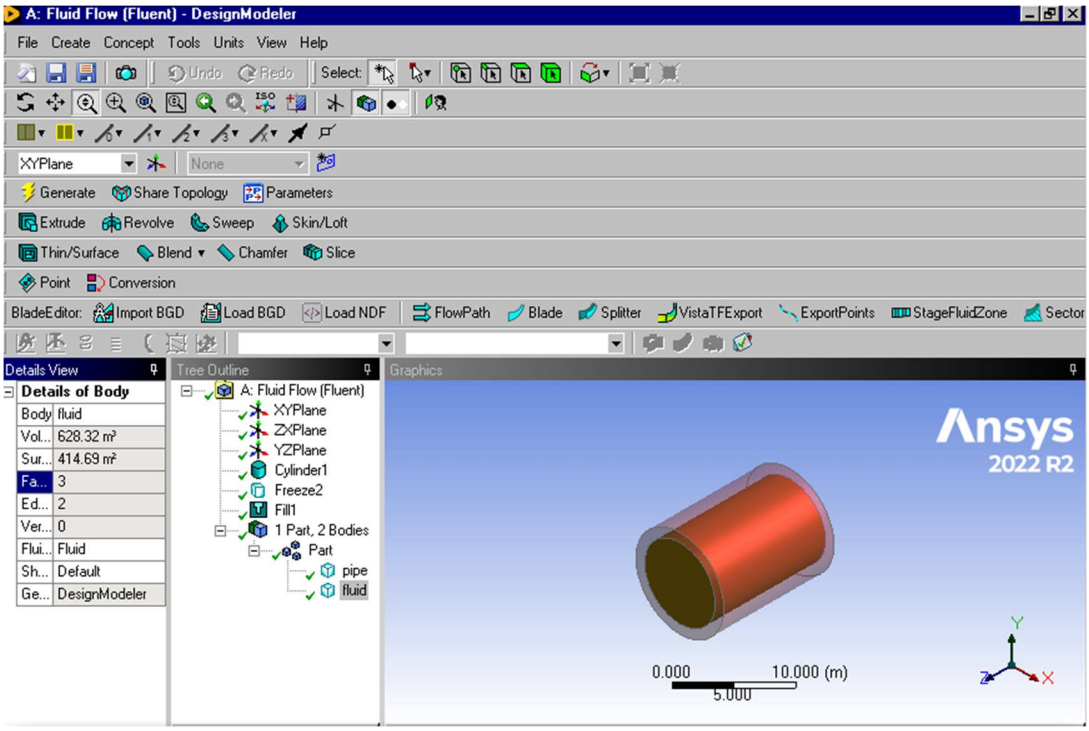

Figure 3.3: A view of an illustrative DesignModeler project.

3.3.3 Mesh

The next step is to mesh the domain, which means dividing the geometry into a number of smaller non-overlapping zones (cells). After opening the meshing tool, and before generating the mesh, we need to specify some preferences and values under "Details of Mesh" box as follows:

- Physics Preference: CFD
- Solver Preference: Fluent
- Under the "Quality" tab; Smoothing: high, Target Skewness: anything equal or more than 0.85

The user may generate the mesh at this step, evaluate its quality and then proceed to manipulate the mesh as required. A view of a meshing window is shown in Figure 3.4.

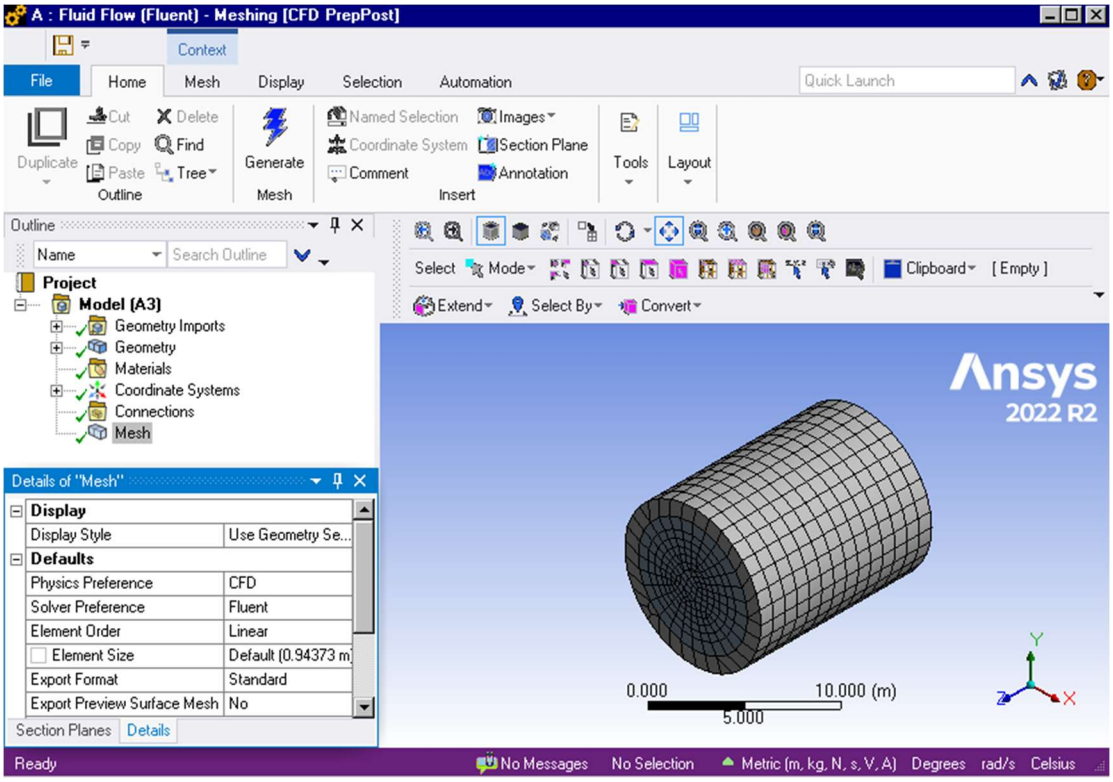

Figure 3.4: A view of the meshing window.

The quality and the fineness of the mesh cannot be evaluated by just looking at the meshed domain, but by checking the details of the mesh. Three of the most important parameters which determine the overall mesh quality are Skewness, Aspect Ratio (Figure 3.5 (a)) and Orthogonal Quality (Figure 3.5 (b)). These three parameters are unitless. A general rule regarding Skewness, “defined as the difference between the shape of the cell and the shape of an equilateral cell of equivalent volume”, is that it should not exceed 0.95 at its maximum and an average value of 0.33 is recommended. Aspect Ratio, “a measure of the stretching of the cell”, is suggested to be kept under 5:1 for bulk flows (not close to the walls),

however, the quadrilateral, hexahedral, and wedge cells inside the boundary layer may be stretched up to an Aspect Ratio of 10:1 without significantly impacting the accuracy of the solution. The Orthogonal Quality, the minimum value resulting from equations (8) and (9), is the third indicator of the mesh quality. The best and worst cells will have this value close to zero and to one, respectively [32]. To ensure that the Solver will not return any errors due to a low-quality mesh, the minimum value of the Orthogonal Quality should not be less than 0.1 and an average value of 0.7 or above is recommended. By setting the "Mesh Metric" and "Display Style" tabs to one of three aforementioned indicators, users can visually check their values and distributions throughout the domain.

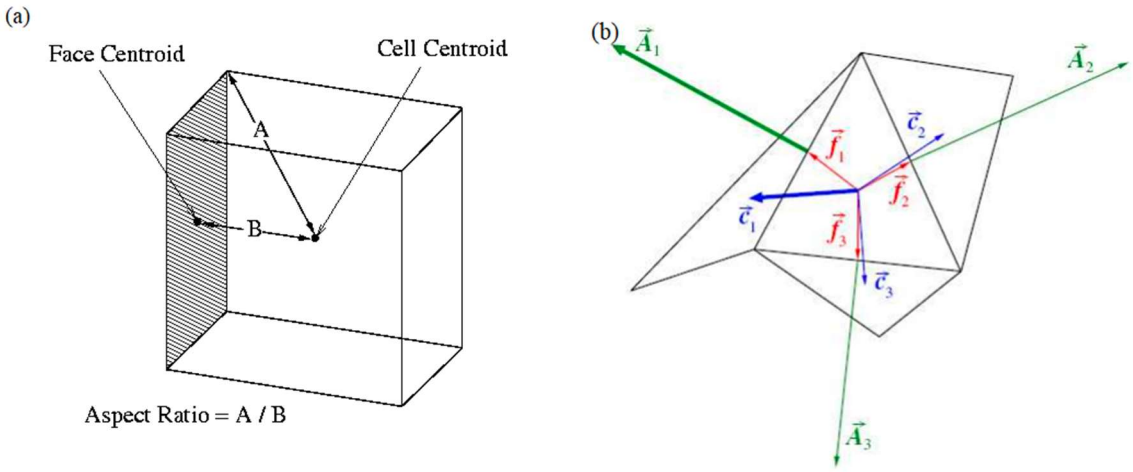

Figure 3.5: (a) Aspect Ratio of a cell zone. (b) Orthogonal Quality [32].

$$\frac{\overrightarrow{A_i}.\overrightarrow{f_i}}{|\overrightarrow{A_i}|.|\overrightarrow{f_i}|} \tag{10}$$

$$\frac{\overrightarrow{A_i}.\overrightarrow{c_i}}{|\overrightarrow{A_i}|.|\overrightarrow{c_i}|} \tag{11}$$

Generally, the fineness of the mesh improves, e.g. higher Orthogonal Quality and lower Skewness, as the number of cells in the mesh increases, thus one of the most common approaches to make a mesh finer is to reduce the element size, which subsequently leads to a higher element count. To do so, the user can either change the "Element Size" located under "Defaults" tab in the details of the mesh box (this will affect the whole domain) or use the "Local Sizing" option which allows to change the size of elements in only some specific zone(s) (this will change the element size only in the selected zones without affecting the unselected zones). When using the latter option, the user needs to right-click on "Mesh" and then select "Sizing" under the "Insert" tab. Other options such as "Method" (to change the type of mesh element, e.g. tetrahedrons, hex dominant, etc.) and "Inflation" (to add inflation layers especially useful at wall boundary conditions) are also accessible under the "Insert" tab.

After achieving an acceptable mesh quality and before proceeding to the setup part, it is often useful to name the different boundaries and zones so that they will be easily distinguishable. This can be done by selecting the boundary or zone of interest, right-clicking and choosing "Create Named Selection".

3.3.4 Solver

After right-clicking on the Setup component, a pop-up window (Fluent Launcher) opens which allows the user to set "The Number of Solver Processes", activate "Double-Precision", check the "Working Directory", etc. Starting the Fluent launcher will open the Fluent window where the user will define the physics of the problem, select from various available models, set the Solver specifications and finally start the

Solver (Figure 3.6). By clicking on each tab under “Outline View”, the available options will be shown inside the “Task Page” window.

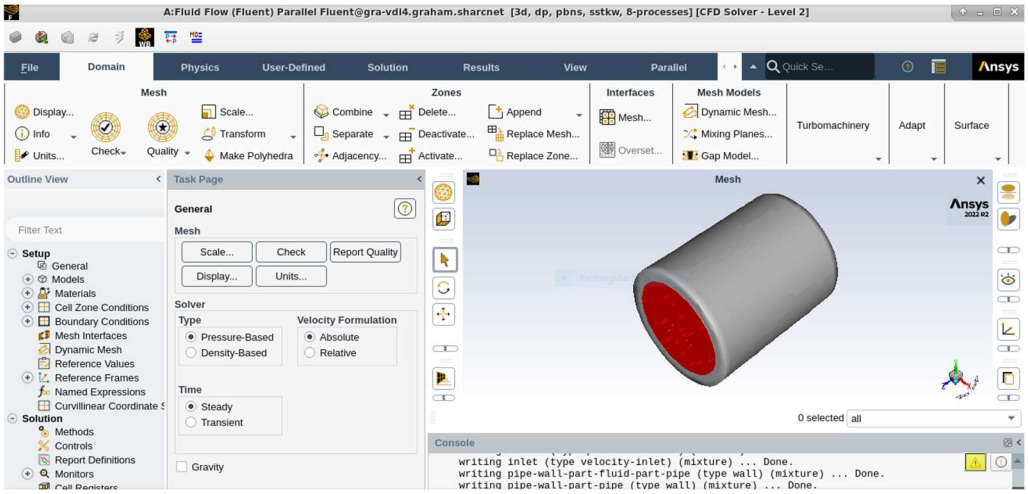

Figure 3.6: A view of a Fluent window.

3.3.4.1 Setup

The Setup task page contains various sections used to define the physics of the problem. These sections, description of their functions, and instructions on how to use them, are discussed in the following:

- General; allows the user to check the Mesh quality, change the units, choose the Solver type (Pressure-Based, for low speed and incompressible flows, or Density-Based, for high speed and compressible flows), select the “Velocity Formulation” (“Absolute”, for cases where most of the flow is not rotating, or “Relative” which is preferred when most of fluid is rotating), set time dependency of the simulation (Steady or Transient), include gravity and specify its value and direction.

- Models; contains the “Multiphase” tab (to activate multiphase models), Energy (should be activated when modeling heat transfer), “Viscous” tab (to choose appropriate turbulence model), “Radiation” tab (to model radiation as well as activating the solar calculator, a feature used for simulating the effect of solar radiation by providing the global positioning and date to the software), “Heat Exchanger”, Species (used for cases when species transport takes place between phases), “Discrete Phase Modeling”, “Eulerian Wall Film” (used to model wall condensation), etc.
- Materials; this tab allows for creating/changing new materials and their physical properties).
- Cell Zone Conditions; to select the type of each cell zone and assign the appropriate material to it.
- Boundary Conditions; to set boundary conditions (velocity at inlet, pressure at outlet, wall boundary conditions) [32,33].

3.3.4.2 Solution

Under the “Solution” tab (Figure 3.6) the user can perform solution settings and calculation tasks:

- Methods; allows the user to specify the Coupling Scheme (SIMPLE/SIMPLEC - generally suggested for laminar flow without additional models activated, PISO - highly recommended for all transient flows and large time steps, Coupled - offers a more robust and efficient single phase implementation for steady-state flows when used with pressure based algorithm), Spatial Discretization (Gradient - used to

discretize the convection and diffusion terms in the flow conservation equations, Pressure - second order, suitable for compressible flows, PRESTO! - suggested for flows with high swirl numbers, high-speed rotating flows, body-force-weighted - for problems with large body forces), Momentum, Energy and Dissipation rate (first or second order - when first or second order accuracy is desired respectively, QUICK - typically more accurate when the mesh structure is aligned with the flow direction, “Third Order MUSCL” - which can improve spatial accuracy for complex three dimensional flows by reducing numerical diffusion).

- Controls; allows the user to set Under-Relaxation Factors, used to stabilize the convergence behavior of the outer nonlinear iterations in the Pressure-Based solver by introducing selective amounts of variable into the system of discretized equations.
- Report Definitions; by accessing this task page the user can define various types of reports such as surface report, volume report, flux report, etc. which are very useful in plotting and monitoring different variables as the solution advances.
- Initialization; under this task page the user can initialize the solution and set initial values (pressure, velocities, energy, etc.), which can be viewed as defining the “zero time” of the simulation.
- Run Calculation; under this tab the user can set the time step size, number of time steps, iterations per time step, etc. and finally start the calculation [32,33].

After starting the calculation, the Solver begins to iterate over the equations and will report the solution advancement, numerically in the Console and visually by plotting the Residual

Values and other variables as defined by the user. When the solution has converged, the user is notified via a message in the Console (Figure 3.7). Another indicator of a converged solution is when the Residuals become straight horizontal lines. After reaching the convergence, the user can either let the calculation finish and cover all physical time of simulation or stop the calculation and proceed to post-processing.

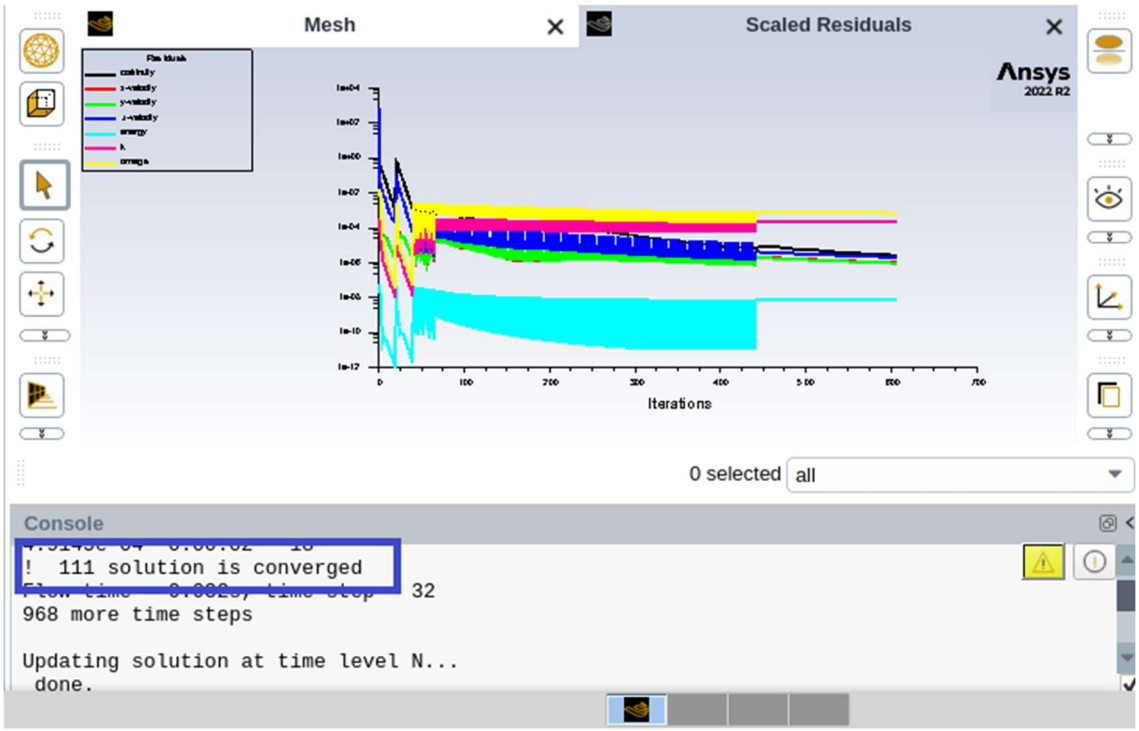

Figure 3.7: User gets notified when the solution is converged.

3.3.5 Results

Once the calculation is completed, the user can start post-processing by accessing the "Results" tab (Figure 3.6) in Fluent. Under this tab, there are various sections to view and analyse the results of the simulation:

- Surface; allows geometrical components to be defined (points, planes, surfaces, etc.) which will be used for data analysis and visualization.
- Graphics; under this tab the user can define options to save and display contours, vectors, path lines and particle tracks.
- Plots; allows the user to plot data in different formats.
- Reports; under this tab the user can perform various calculation tasks such as computing fluxes, forces, surface, and volume integrals.
- Animation; allows animations to be generated (before generating, animations need to be defined under "Solution" tab before starting the calculation).
- Model specific; this tab contains data processing and visualization options related to specific models activated for simulation.

In addition to the data processing options accessible in the solution component of a Fluent project, some further options are located in the "Results" tab (Figures 3.2 and 3.8).

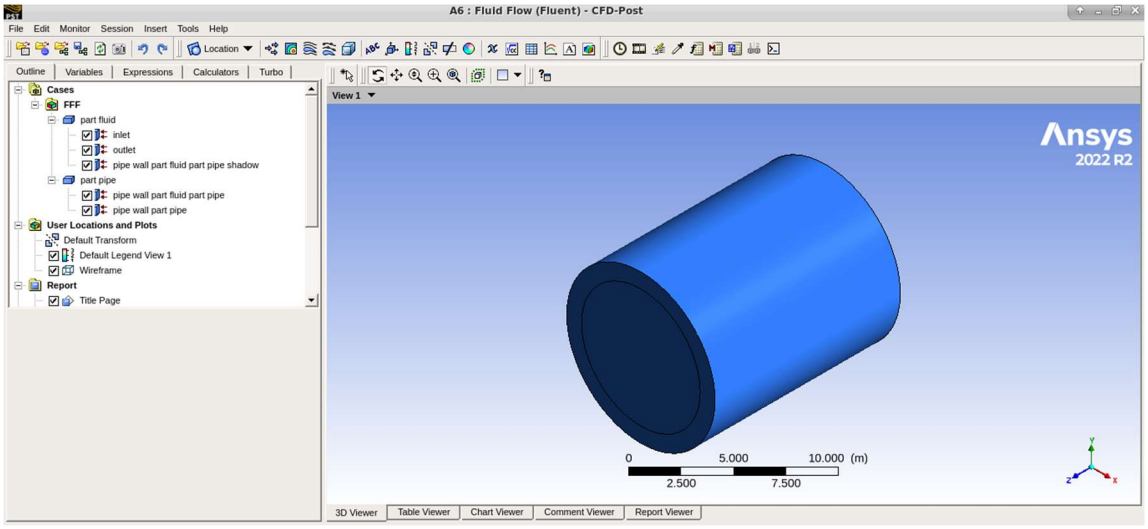

Figure 3.8: A view of Results window, used for post-processing of a Fluent project.

- Taskbar; includes various options such as location (same as surface option in the last section), contour definition and plotting, particle tracking, volume rendering, etc.
- Outline; the user can perform general tasks such as selecting different zones of the domain to be displayed, setting the position of the graphs' legends, titles, etc.
- Variables; under this tab the user can change the units of different variables, minimum and maximum values for display in the contours and calculations.
- Expressions; allows the user to create and change expressions to be used for post-processing.
- Calculators; contains Macro, Mesh, and Function calculators which allows the user to perform various calculations such as fan noise, maximum face angle (in mesh), torque, etc. as needed.
- Turbo; includes specific options related to turbo machinery post-processing.

3.4 Models Investigated in This Work

There were various models and options available in ANSYS Fluent related to this research. Four scenarios were investigated both in 2D and 3D and after careful consideration one of them was selected to conduct our investigations in more details. A

general description of what was of interest in this study as well as the four scenarios tested is discussed in the following sections:

3.4.1 General Description of the Model

The aim of this work was to develop the computational knowhow using ANSYS Fluent to model the heat transfer process of four-season greenhouses in an attempt to one day be able to optimize the design of the GAHT[1] system. The general design of the model used in this work consisted of an above-ground structure (a rectangle/square in 2D or a rectangular prism/cube in 3D), under-ground soil (follows the same shape as the above-ground structure, but with less depth/height), a pipe or a group of pipes passing through the soil and connecting the two corners of the greenhouse together (Figure 3.9).

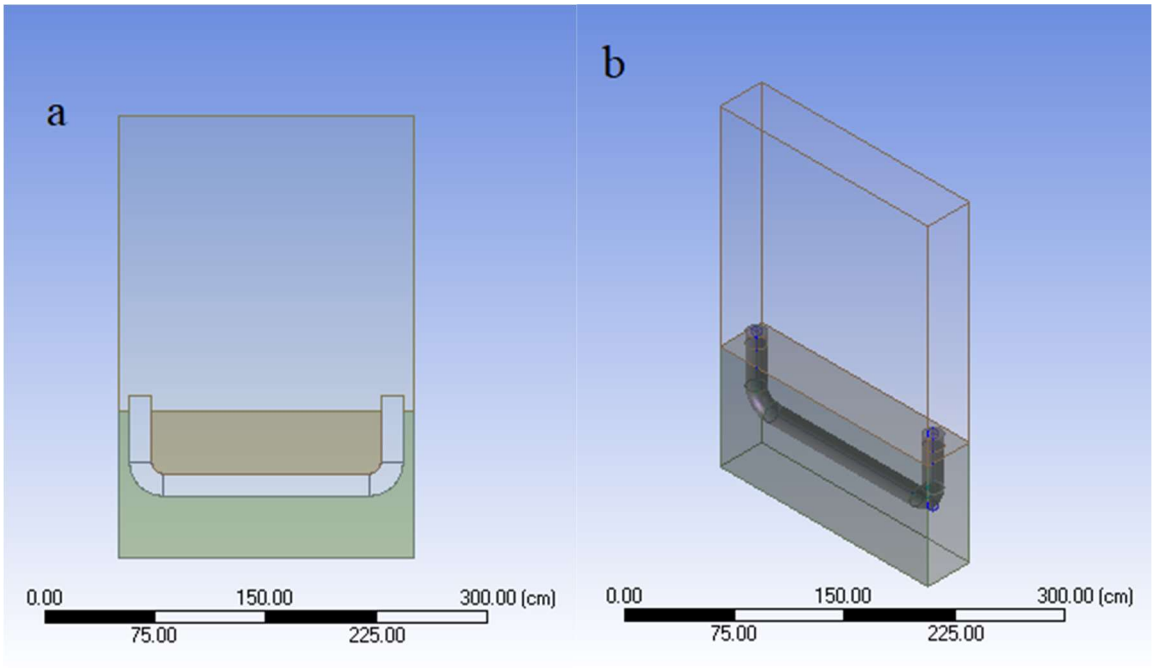

Figure 3.9: Geometry of the model; a) 2D, b) 3D.

[1] Ground to Air Heat Transfer.

At the entrance of the pipe in the corner of the greenhouse, a “fan boundary condition” forces the air into the pipe. In the pipe the air thermally interacting with the soil before it reenters the greenhouse at the other corner. By repeating this process during the daytime, the air temperature gets regulated [cooling] as it stores its excess heat in the soil. During the nighttime when the air temperature is cooler in the greenhouse, heat is extracted by the air from the ground during the circulation process. This approach not only prevents energy from being wasted during the cooling process but also reduces if not eliminated the need for external heating. In addition to convection heat transfer, the aim was also to model the heat transfer which occurs during the phase change, a result of warm humid air meeting the colder soil. When hot moisture carrying air passes through the colder pipe, the vapor in the air condenses and forms liquid water thereby releasing latent heat into the ground due to the phase change.

3.4.2 Soil as A Porous Medium

Soil consists of five constituents: minerals, soil organic matter, living organism, gas, and water [34]. The overall composition of soil can be viewed as having two parts: a solid matrix and empty spaces or holes. The solid matrix is usually stable and not moving, but the empty spaces are open for the penetration of gas or liquid, thus soil can be viewed as a porous medium. It is possible to model porous media and study associated phenomena in ANSYS Fluent, however there are limitations forced by the software which the user should consider carefully before investing too much resources on this model. Some of these

limitations are reporting a "superficial velocity"[2] instead of a real velocity, a porous zone is isotropic in all directions, the effects of the porous zone on turbulence are approximate, no interaction between the porous region and shock wave is considered, etc. [32].

Considering the above, modeling a realistic geometry of a porous material could be extremely difficult, if not impossible, and even if the user manages to design such a geometry, meshing that domain would demand extraordinarily high resources that could make the whole project unmanageable. In ANSYS Fluent, to model a porous medium, the user starts by designing the geometry and considering porous medium as a simple fluid domain. The meshing is also the same as with other nonporous media, but it is in the "Setup" of the project where the user defines the "Porous Zone" and sets the required parameters. In the "Setup" section and under the "cell zone conditions" tab, the user can activate the "porous zone" tab by editing the cell zone (Figure 3.10).

[2] The porous region in ANSYS Fluent is not actually porous, it is a fluid zone 100% open to the flow and as the flow enters porous zone, the software supresses velocity and pressure of the flow, this supressed/reduced velocity is called "superficial velocity" and is calculated based on volumetric flow rate. In the governing equations, it is represented as below [32]:

$$\vec{v}_{superficial} = \gamma \vec{v}_{physical}$$

"where γ is the porosity of the media defined as the ratio of the volume occupied by the fluid to the total volume" [33].

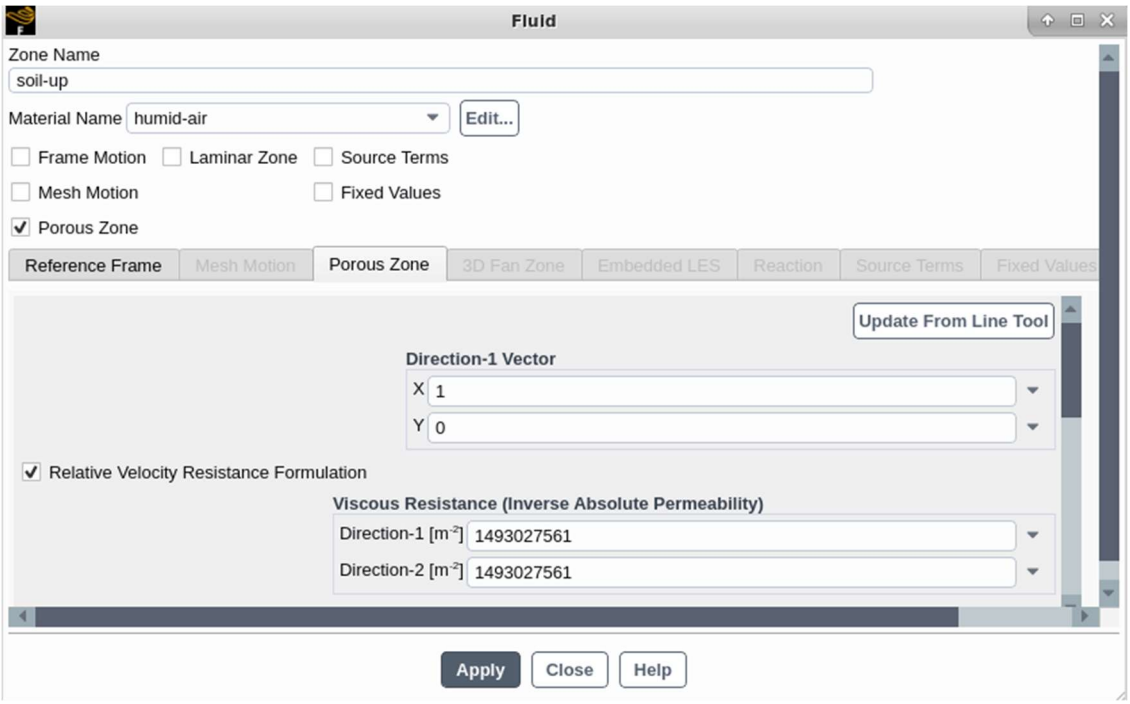

Figure 3.10: A "porous zone" tab in a Fluent project.

After activating the porous formulation, the user can proceed to set the necessary parameters. ANSYS Fluent treats a porous zone as a special type of fluid zone where the software imposes a velocity/pressure drop to the flow to compensate for the lack of physical blockage being present in the porous region [32].

In addition, the user needs to set the fluid porosity and two sets of coefficients (viscous and inertial resistance) for the porous region. If simulating a porous material manufactured by other producers, these coefficients can be obtained by contacting the manufacturer, otherwise the coefficients need to be calculated/experimentally measured by the user with details of the available methods and assumptions available in the Fluent user's guide [32].

There are two thermal models available for porous regions: *Equilibrium* and *Non-equilibrium*. When using the thermal equilibrium model, the software considers there is thermal equilibrium between the solid structure of the porous region and the fluid passing through the empty spaces, thus no heat transfer between the porous material and the fluid can be modeled. When using thermal non-equilibrium model, however, the software will account for the thermal interaction between the solid structure of the porous zone and the fluid passing through voids. As mentioned previously, Fluent treats the porous zone as a special type of fluid zone, but when the user activates the non-equilibrium model, Fluent will generate an additional cell zone to represent the solid part of the porous medium. This cell zone is identical to the fluid zone and is spatially coincident with it. Further details and information on modeling porous regions in Fluent can be found in Fluent users' guide, section 7.2.3 [32].

One important limitation imposed when using the thermal *non-equilibrium* model in a porous zone is that this model is not compatible with any of the multiphase models (Volume of Fluid, Mixture and Eulerian multiphase models) in Fluent [32]. In other words, user may model multiphase flows in porous regions only in conjunction with *Equilibrium* thermal model (meaning that no heat transfer between the flow and solid structure of porous zone would be accounted for). So in this work if it was decided to model the phase change due to heat transfer (multiphase model), it would become impossible to activate *Non-equilibrium* thermal model (which would mean neglecting the heat transfer between the fluid and soil solid structure). In addition, this would prevent the change in heat due to vapor condensation from being included in the energy calculations. Because of these factors

it was concluded that although greenhouse soil is in fact a porous medium, neglecting the porosity effects in the soil creates fewer errors in our simulations, than of modeling soil as porous medium and instead neglecting the condensation.

3.4.3 Surface Condensation with Eulerian Wall Film Model

As mentioned in a previous section, the daytime air inside the greenhouse is hot and humid. When this air gets circulated inside the pipes embedded in the colder soil below the greenhouse, some of its vapor content condenses and forms liquid water which subsequently release latent heat into the pipe/soil. Therefore, one important phenomenon which needed to be modeled in this research was the vapor to liquid phase change. One of the available models in ANSYS Fluent for simulating this phase change is the "Eulerian Wall Film", used to model the formation and flow of thin liquid films on the walls of surfaces. Like other models, Eulerian Wall Film (EWF), has its own advantages, disadvantages, and limitations. Some limitations of the EWF model are: this model is only available for 3D geometries, it accounts only for surface condensation, not bulk condensation, in order for have this model to interact properly with other models (VOF multiphase or radiation), the boundary conditions must be modified using User Defined Functions, and lastly the EWF model cannot be used for moving or deforming meshes [32].

To enable the EWF model, the user should access its setting under the "Models" tab in Fluent (Figure 3.11). After checking the box, the dialog box expands and displays additional model and setup options. Checking the first three boxes under the "Solution Options" will instruct the software to solve related equations for momentum, energy, and scalar transport. "Phase Coupling", located under "Solution Options" (Figure 3.11), enables

the phase change between the film material (liquid) and the gas species (vapor) through condensation or evaporation. It also computes secondary phase collection efficiency on a wall surface and enables the interaction of EWF with the VOF multiphase model. “Treat Sharp Edge” option determines how the film wall edge is treated when the “edge angle” is smaller than the “sharp edge angle”, in other words, it determines whether the film becomes detached from the wall or film bends around the edge while still being attached to the wall.

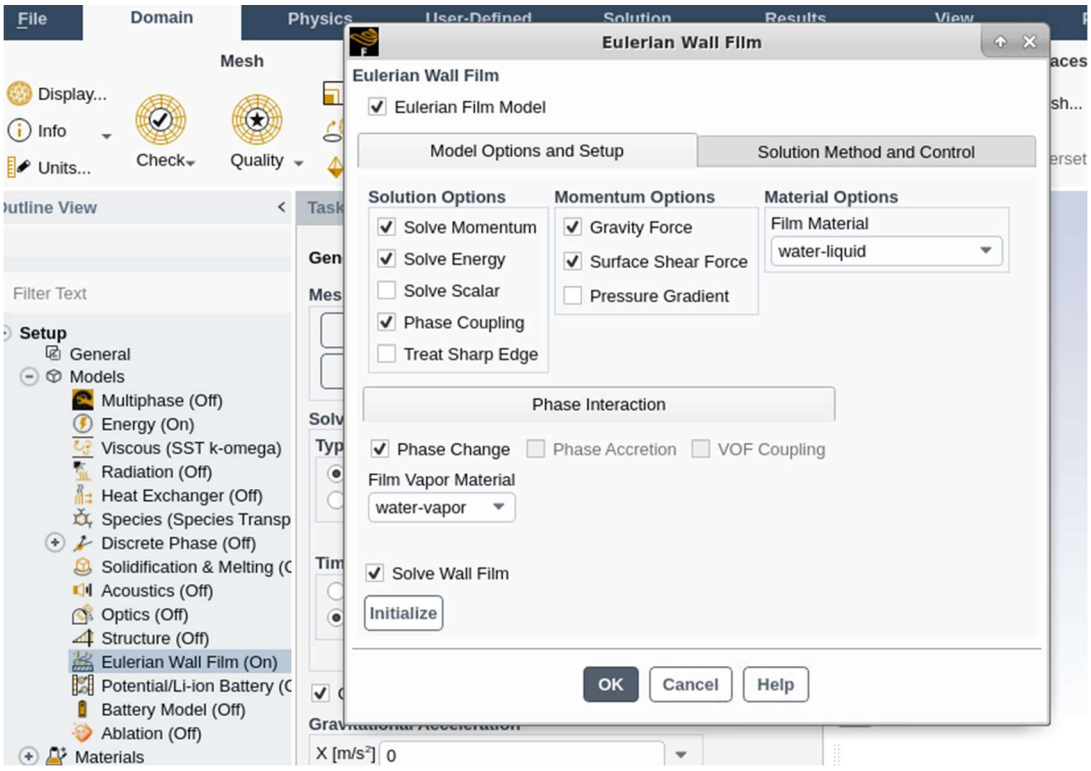

Figure 3.11: Eulerian Wall Film settings window.

Under the “Momentum Options” (Figure 3.11), “Gravity Force” and “Surface Shear Force” cause the film to accelerate in the direction of the gravity component parallel to

the wall and in the direction of external flow, respectively. “Pressure Gradient” (Figure 3.11) is responsible for accelerating the film in the direction opposing the “gradient in external pressure”[3]. After checking the “Phase Change” box, the user can set the film material (liquid phase) and film vapor material (gas phase).

Under the “Solution Methods and Controls” tab, the user can perform additional tasks related to EWF such as selecting discretization methods, setting the maximum film thickness (beyond which the material gets removed from the film if exceeded), and also specifying the model specific time step controls. Further information and instruction on how to set and use the EWF model can be found in Fluent users’ guide, chapter 25 [32].

As mentioned previously, the EWF model is only available for 3D geometries. On the other hand, to achieve a convergent solution and obtain accurate results, it was necessary to have a sufficiently fine mesh (e.g. 125 million cells), which for 3D geometries led to extremely long times to reach convergence and were computationally costly. As a result, no further simulations were conducted using this model.

3.4.4 Phase Change Using Mixture Multiphase Model

ANSYS Fluent features three multiphase models, Volume of Fluid (VOF), Mixture, and Eulerain model. The Mixture multiphase model is capable of modeling ***n*** phases, and solves the momentum, energy, and continuity equations for the mixture phase, the

[3] External Pressure Gradient describes the direction in which the fastest growth of pressure takes place. The thin film moves from areas with higher pressures to areas with lower pressures, which is opposite to the direction of pressure gradient vector.

volume fraction equations for the secondary phase(s), and the algebraic expressions for the relative velocities. This model has the following limitations:

- It is only available for the Pressure-Based solver and is not compatible with the Density-Based solver.
- Only one of the phases may be defined as a compressible ideal gas, but unlimited number of compressible liquids can be modeled using appropriate UDFs.
- It can not be used in conjunction with Solidification or Melting models.
- It can not be used when "Streamwise Periodic Flow" with "Specified Mass Flow Rate" is used.
- This model does not allow for inviscid flows[4].
- The Singhal et al. cavitation model, available with the Mixture model, is not compatible with the LES[5] turbulence model.
- The relative formulation should not be used in combination with the MRF[6] and Mixture model.
- When using the Mixture model in combination with the DPM[7] model, the "Shared Memory" method can not be used [32].

In Fluent, multiphase modeling can be activated by accessing it under "Models" and checking the box for the model of choice. After activating the Mixture model, the

[4] A flow with zero viscosity, such a flow has no internal friction and does not show resistance against deformation.
[5] Large Eddy Simulation (LES) is a mathematical model for turbulence used in CFD.
[6] Multiple Reference Frames.
[7] The Discrete Phase Model.

multiphase box expands and reveals further options of the model to be set by the user (Figure 3.12).

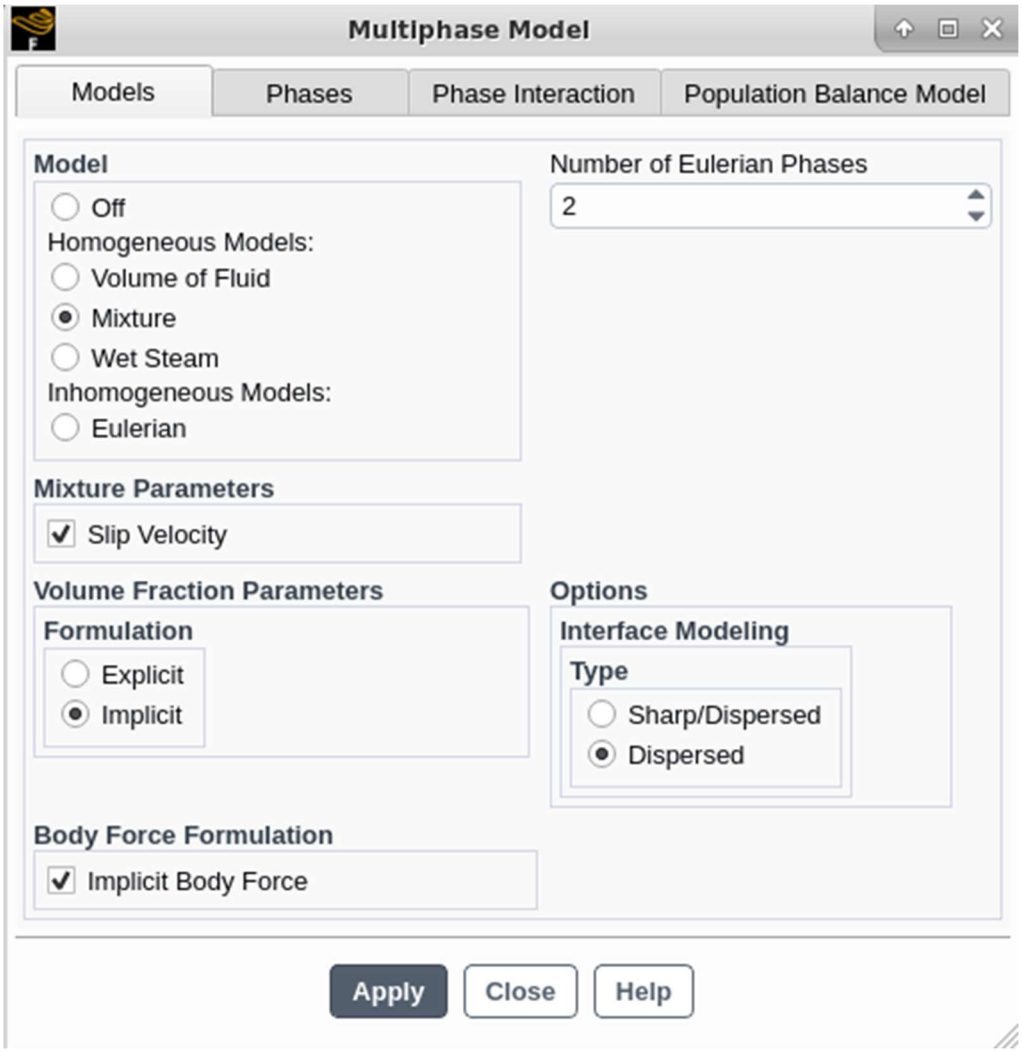

Figure 3.12: Mixture multiphase model settings window.

After enabling the Mixture model, the user can choose the number of phases (two or more), activate/deactivate the "Slip Velocity" option which enables/disables calculation of "Slip Velocity" for the secondary phase, choose Explicit/Implicit

schemes to be used by the Solver, activate “Implicit Body Force” which instructs the Solver to account for partial equilibrium of the “Pressure Gradient” and “Body Forces” in the “Momentum Equations” and generally improves solution convergence, and lastly select the type of “Interface Modeling” as appropriate to the model.

Under the “Phases” tab, the user can assign desired material to each phase and also edit the material properties if needed. The “Phase Interaction” tab contains three sub-tabs “Forces”, “Heat, Mass, Reactions” and “Interfacial Area”. The “Forces” tab contains settings for Drag, Slip Velocity, and Surface Tension between the phases that depends on the existing phases and should be set specifically for each problem. Under the “Heat, Mass, Reactions” tab the user can specify which type of Heat/Mass transfer and reactions take place in the problem. To activate phase changes, the user should define one “Mass Transfer Mechanism” under “Phases Interaction” tab (Figure 3.13). For example, to model condensation of water vapor, the settings should be as follows: it takes place from the liquid phase (phase-1) to vapor phase (phase-2) through evaporation/condensation mechanism and the species should be set as “h2o”.

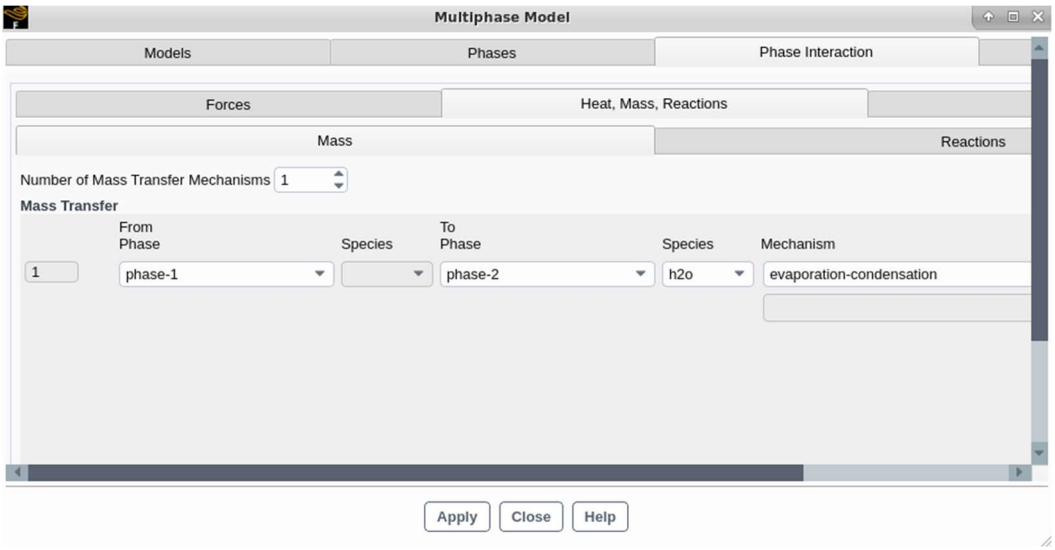

Figure 3.13: Phase interaction settings window in Mixture multiphase model.

Unlike EWF, the Mixture model can be used for both 2D and 3D geometries. Phase change was modeled using the Mixture multiphase model for both geometries and the solutions successfully achieved convergence. Unfortunately, as in the EWF case, due to size of 3D simulations, it was decided to proceed only with a 2D geometry. In the next chapter, a deeper look at this model will be taken and the details of the simulations presented.

Chapter 4 Our Simulation Settings and The Results

4.1 Geometry

Our simulations were performed with a 2D geometry. The greenhouse chamber above the ground was represented by a square with sides 2 meters in length. The soil beneath the greenhouse chamber was a rectangle with a length of 2 meters and a depth of 1 meter. A 2D pipe with a wall thickness of 1 millimeter and a diameter of 15 centimeters (excluding walls) starts from one side of the chamber, enters the soil and exits from the other side. The longest vertical distance between each entrance of the pipe and the lower wall of pipe's horizontal segment was 67.5 centimeters. The longest horizontal distance between the vertical segments of the pipe was 185 centimeters. 10 centimeters from each vertical segment of the pipe was located above the ground inside the chamber (see Figure 4.1). It should also be mentioned that this method of modeling the pipe in 2D is not unique to the pipe, since both pipe and channel in 3D are represented the same way when modeled in 2D, so this geometry could be viewed as representing a pipe or a cubical channel with a square side equal to the diameter of the pipe.

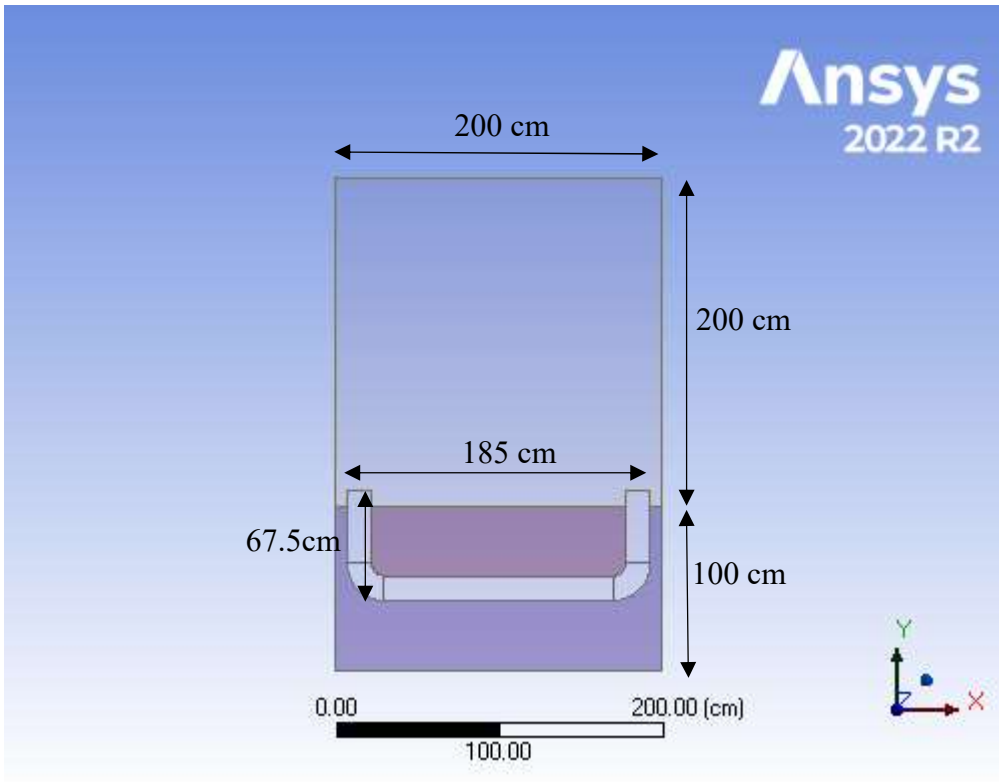

Figure 4.1: Geometry of the computational domain used in this work. A square with sides 2 meters in length represents the greenhouse chamber while beneath is a rectangle 2 meters in length and 1 meter in depth which represents the soil domain. A 2D pipe with a wall thickness of 1 millimeter and a diameter of 15 centimeters enters the soil on one side and exits from the other side.

4.2 Mesh

The mesh used in this work had an element count of 74727 and a node count of 75262. The element size was chosen to be 9 millimeters and the mesh *Defeaturing Size*[8] was 4.5×10^{-5} meters. A *Curvature Minimum Size* [9] of 9×10^{-5} meters was applied. These

[8] When enabled, the features with size equal or smaller than the Defeaturing Size will be removed automatically [32].
[9] Is the minimum size returned to the mesher [32].

characteristics resulted in a fine mesh with average values of 9.3551×10^{-3} and 0.99883 for skewness and orthogonal quality respectively.

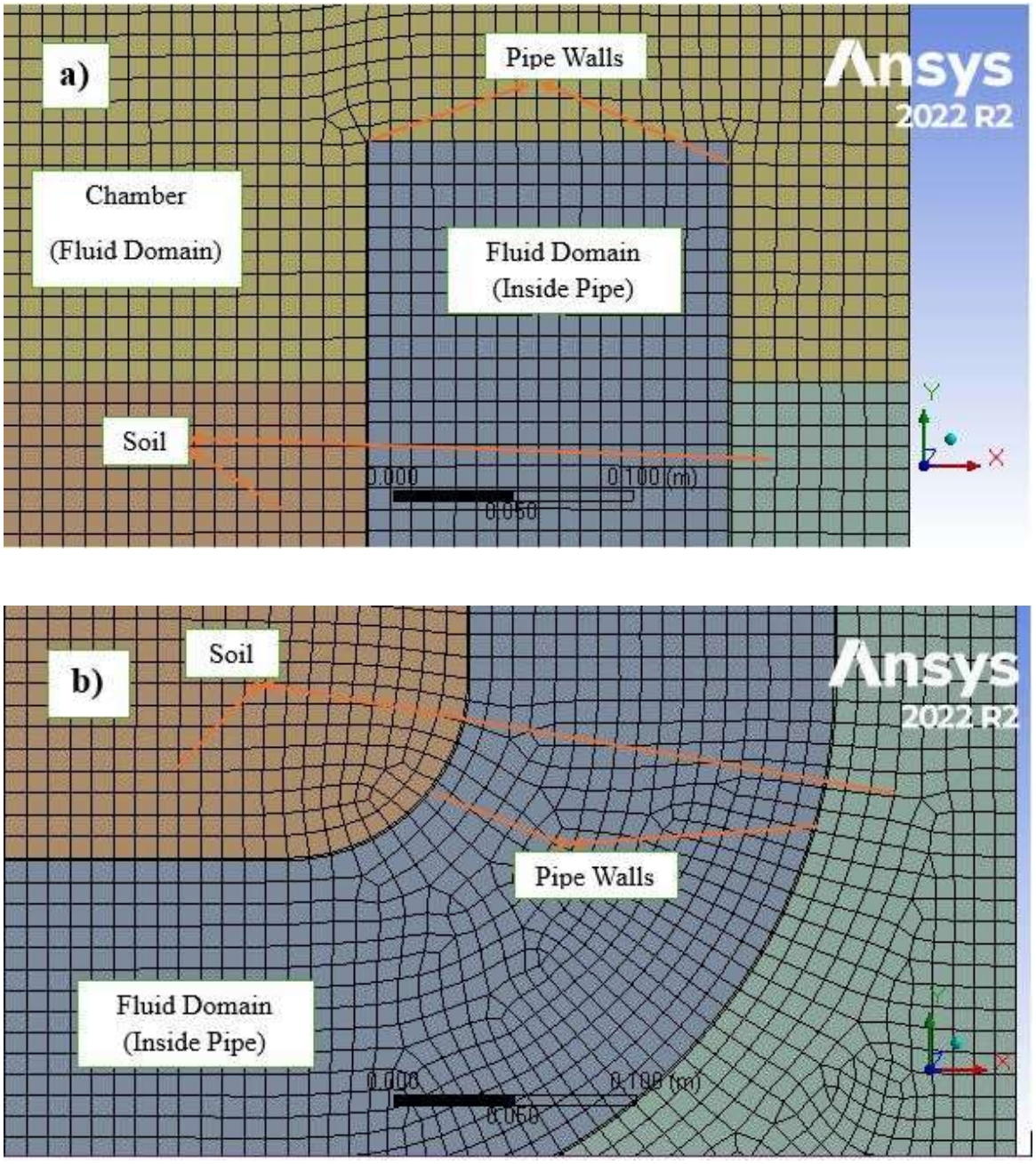

Figure 4.2: Meshed computational domain, a) at the area when pipe exits the soil and enters the chamber, b) at area inside the soil where pipe is bent.

4.3 Setup

This section includes the details of the modeling. The pressure-based solver with absolute velocity formulation and transient time dependency was used. A gravitational acceleration of 9.81 m/s^2 was applied along the negative *y*-axis to account for the effect of earth's gravitational force. The "Energy Equation" in Fluent was turned on because modeling heat transfer through convection and phase change was intended to be included in the model. Because of the importance of wall heat transfer in this work, the SST k-omega viscous model was used for better near wall treatment. Since the humid air in the gas phase had more than one species, air and water vapor, the "species transport" option was used. The materials used in this work were: humid air (consisting of water vapor and dry air), liquid water (condensate), soil, and copper (for the pipe). As mentioned previously, the multiphase model used in this work was the Mixture Multiphase Model. A UDF[10] was also compiled to the Solver to calculate the saturation temperature of vapor (the temperature at which condensation and phase change take place) based on the partial pressure of the water vapor to improve the accuracy of the results of the solution. The soil and pipe walls were set as solid zones indicating that the space inside the chamber and inside the pipe were defined as fluid zones. Regarding the boundary conditions, the chamber and soil outer walls were set to be isolated from the surrounding environment (zero thickness and zero heat flux). At the entrance of the pipe on the left side, an "internal fan" boundary condition was defined, which allowed for a pressure jump to be applied to the fluid flow when it passed

[10] Refer to appendix A for details.

through the fan. The PISO[11] scheme, highly recommended for all transient flows, was used for the pressure-velocity coupling algorithm with a skewness and neighbor correction of 1. For spatial discretization, the PRESTO! scheme was used for pressure while first order upwind was applied to the rest of the variables (momentum, volume fraction, energy, etc.). For the solution control part, default values were used and solutions were initialized using the standard initialization method. After initialization, the specific values (RH of humid air, initial temperatures of the flow, soil, and pipe) were patched for each case as required and a time step value of 0.001s was set for all cases.

As discussed previously, one of the objectives of this study was to model and study the heat transfer between air and soil. This process can occur in two directions: from hot air to cold soil (in the summer and during the day), and from hot soil to cold air (in winter mostly during the night). For the case of hot air and cold soil, the initial air temperature was set to 35 °C and the temperature of soil and pipe as 15 °C. To test the overall performance of the model, simulations were first conducted with a simplified boundary condition of RH = 0 (representing dry air). This could also provide the conditions for a comparison between two cases involving dry and humid air, which will be discussed later in section 4.4.2.1. The case of dry air was relatively simple, since no phase change would take place for such a situation and therefore was done first. Following this, humidity was added to the air and the simulations were repeated. An RH of 80% was selected, since that is the optimal operating value for greenhouses during the day. The simulations were performed until thermal equilibrium or near equilibrium point was reached (typically at some point between 500s

[11] Pressure-Implicit with Splitting of Operators.

and 600s of physical time). At the end of each simulation, the properties of the soil (average temperature, total energy, and enthalpy) were extracted and used as the initial conditions for the simulations involving hot soil and cold air. For this case, the purpose was to reproduce the situation in a greenhouse during the night so the initial temperature of the air was set as 15 °C with 50% RH. The simulations were conducted until thermal equilibrium or near equilibrium point was reached. In order to investigate the effects of the fan speed on the heat transfer rate, simulations were conducted using three different fan pressure jump values: 30, 60, and 120Pa (which are equivalent to average flow velocities of around 6, 8 and 12 m/s at the fan in the negative *y*-axis direction). The results are presented in the next section.

4.4 Results

4.4.1 Dry Air

For these simulations, the hot dry air initially set to 35 °C was circulated through the pipe for 100s. The initial temperature for both the soil and the pipe was 15 °C. The summary of these simulations for three different fan pressure jump values are presented in Table 4.1.

Table 4.1: Results of simulations conducted when hot dry air initially set to 35 °C was circulated through a pipe surrounded by soil with an initial temperature of 15 °C for 100s.

Fan Pressure Jump	30Pa	60Pa	120Pa

Air T_i	35 °C	35 °C	35 °C
Solid* T_i	15 °C	15 °C	15 °C
Air Total E_i	-3.94 × 10^5 J	-3.94 × 10^5 J	-3.94 × 10^5 J
Solid Total E_i	1.33 × 10^9 J	1.33 × 10^9 J	1.33 × 10^9 J
Fan Velocity in y-axis Direction	-5.99 m/s	-8.51 m/s	-12.07 m/s
Air Avg T_f	15.98 °C	15.62 °C	15.48 °C
Solid* Avg T_f	15.018 °C	15.018 °C	15.018 °C
Air Total E_f	-4.62 × 10^5 J	-4.64 × 10^5 J	-4.65 × 10^5 J
Solid Total E_f	1.33 × 10^9 J	1.33 × 10^9 J	1.33 × 10^9 J
Air ΔT	-19.02 °C	-19.37 °C	-19.52 °C
Solid ΔT	0.018 °C	0.018 °C	0.018 °C
Air ΔE	-6.87 × 10^4 J	-7.02 × 10^4 J	-7.16 × 10^4 J
Solid ΔE	6.87 × 10^4 J	7.02 × 10^4 J	7.15 × 10^4 J

*Solid is used to refer to both soil and pipe together.

For the geometry used in this work, the total mass for the air and soil were 4.93 kg and 3556 kg respectively. The value used in this work for the specific heat (C_p) of soil was 1309.7 J.kg/K and 1006.4 J.kg/K for air. Because the mass of the soil was so much larger than that of the air, the effects of energy exchange between air and soil had a much larger effect on the air temperature compared to the soil temperature. As a result, when a given amount of energy is lost by the air and added to the soil, the temperature of air will drop dramatically whereas the temperature of the soil might only change within a few decimal

points. For this reason, the air and soil temperatures are represented with three decimal points in Table 4.1.

As the data in Table 4.1 show, the circulation of hot dry air through the pipe caused the transfer of thermal energy from the air to the soil resulting in a temperature rise in the soil and temperature drop in the air. The data also show that there is small but positive correlation between fan velocity and the amount of energy transferred, meaning that higher fan velocities resulted in more energy transferred from the air to the soil. The two bottom rows of Table 4.1 show that, for each fan velocity, the amount of energy added to the solid (soil and pipe) was (with very good accuracy, less than 0.15% uncertainty) equal to the energy lost by air therefore satisfying the conservation of energy. Figure 4.3 shows the changes in air and solid temperatures over a period of 100 seconds.

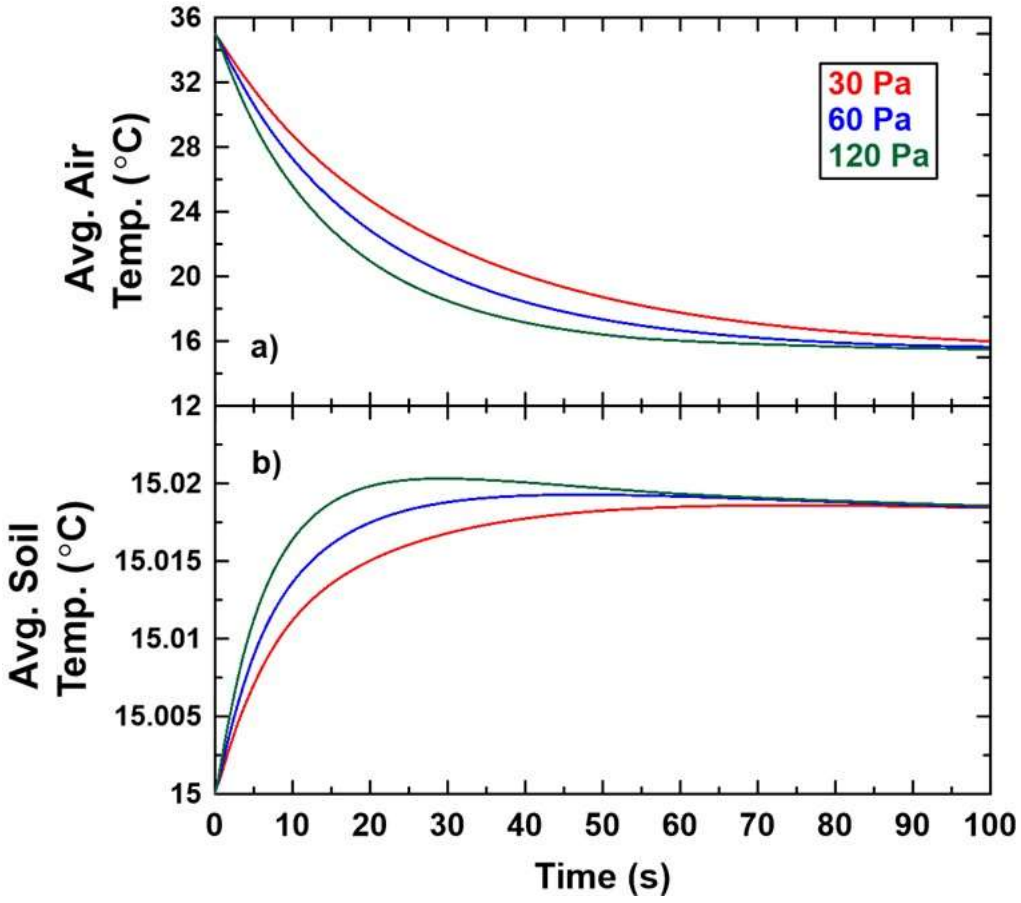

Figure 4.3: Average temperature of a) dry air, and b) the solid (referring to soil and pipe domain together).

Figure 4.3 a) shows that for all values of fan pressure jump, the average temperature of air is decreasing indicating the transfer of heat from the hot air to the cold soil. It can also be observed that, throughout the simulation time, the rate of temperature drop is decreasing (curves are becoming flat) for all three fan velocities. This is expected, since at the beginning of the simulation the difference between the temperature of air and soil is at a maximum and so is the rate of heat transfer from hot air to cold soil. As time passes, due to

the transfer of thermal energy from the air to the soil, the difference between the air and soil temperatures becomes smaller which decreases the rate of heat transfer. Figure 4.3 a) also shows that, at any time throughout the simulation, the average temperature of air is smaller for greater fan pressure jump values. In other words, greater fan pressure jump values lead to a faster temperature drop in the air (which indicates higher rate of energy loss in the air). This is due to the fact that higher fan pressure jump values mean a higher rate of mass transfer, which means a higher rate of heat transfer as well. Figure 4.3 b) shows a common pattern in the average temperature of the solid for all three fan pressures. As the simulation begins, the temperature of the solid rises reaching a maximum value followed by a small decrease in temperature. It can also be observed that, for higher fan velocities, the maximum temperature is reached faster than for lower fan velocities. As discussed previously (for temperature of air), higher fan velocity facilitates the process of heat transfer causing the temperature of the soil to increase more rapidly. From a decrease in temperature it might be expected that the energy of the soil also undergoes a similar behavior. Figure 4.4 shows the change in energy of the soil as a function of time for the three fan pressures considered in this work. As can be seen the change in energy of the solid increases monotonically until it eventually begins to level off indicating that the soil is absorbing less energy from the dry air. One possibility for the small increase and decrease in the average temperature of the solid shown in figure 4.3 b) may be due simply to the diffusion of heat in the soil.

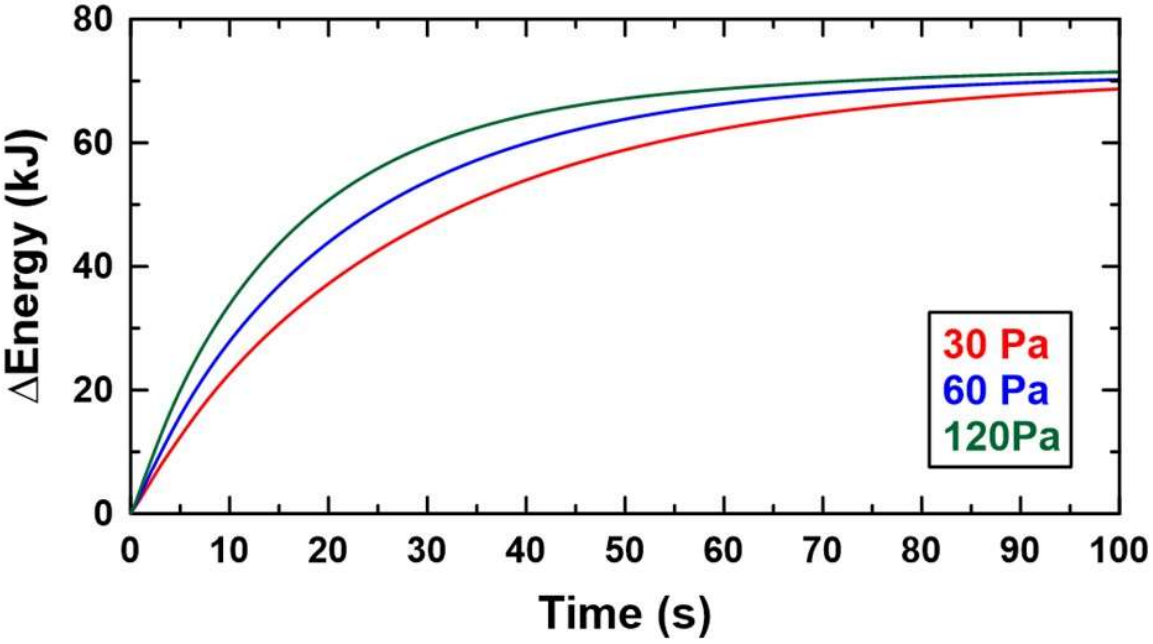

Figure 4.4: a) The change in energy of the soil for the three fan pressures (30 Pa (red), 60 Pa (blue), 120 Pa (green)).

4.4.2 Humid Air

For this part, water vapor was added to the gaseous phase making the RH of humid air equal to 80% at the beginning of the simulation. For better accuracy in modeling the phase change (condensation), a UDF was added to the mixture multiphase model. This UDF, presented in Appendix A, was written to calculate the saturation temperature of water vapor, at which condensation happens, according to the partial pressure of vapor.

4.4.2.1 Hot Humid Air and Cold Soil

For this case, hot humid air initially at 35 °C with 80% RH (equivalent to an H_2O mass fraction of 0.0281 at 35 °C) was circulated through the pipe for 600s. The initial temperature for both the soil and pipe (reported as "solid") was 15 °C. The summary of these simulations for three different fan pressure jump values is presented in Table 4.2.

Before proceeding to Table 4.2, it should be noted that the multiphase model used in this work (Mixture model) solves only one set of energy equations for the mixture as a whole which contains all the phases in the fluid domain (in this case humid air and liquid water). Therefore, when using the Mixture multiphase model in Fluent, it is not possible to track energy changes for each phase of the mixture separately. Energy and temperature values reported in Table 4.2 for the mixture (humid air and liquid water together) refer to the bulk energy and bulk temperature of the mixture. Liquid and gaseous phases both contribute to the energy and temperature of the mixture, however, it is not possible to know the contributions of each phase individually. That is the reason for which, unlike for the case of dry air, the amounts of energy lost by the components of the mixture are not equal to the energy added to the solid. For simulations involving dry air, energy lost by dry air could only be transferred to the solid zone, but when there is humidity present in the fluid domain, liquid water (generated as a result of condensation) can thermally interact with the gaseous phase and with the solid zone. For simulations involving more than one phase in the fluid domain it is only possible to track the energy and momentum changes for the mixture and that is why the energy and temperature values shown in Table 4.2 and Figure 4.5 are reported for the "mixture" (humid air and liquid water together), and not for each

component separately. For the data reported in Table 4.2, the fluid domain initially contains only the gaseous phase (humid air), but in the final state there are gaseous and liquid phases in the fluid domain which are together reported under the label “mixture”.

Table 4.2: Results of simulations conducted when hot humid air initially set to 35 °C and 80% RH was circulated through a pipe surrounded by soil with an initial temperature of 15 °C.

Fan Pressure Jump	30Pa	60Pa	120Pa
Air Avg T_i	35 °C	35 °C	35 °C
Air RH_i	80%	80%	80%
Solid* Avg T_i	15 °C	15 °C	15 °C
Air Total E_i	-2.26 × 10^6 J	-2.26 × 10^6 J	-2.26 × 10^6 J
Solid Total E_i	1.33 × 10^9 J	1.33 × 10^9 J	1.33 × 10^9 J
Fan Velocity in Y Axis Direction	-6.04 m/s	-8.59 m/s	-12.22 m/s
Mixture Avg T_f	15.78 °C	15.79 °C	15.82 °C
Air RH_f	0.0012%	0.0015%	0.00096%
Solid* Avg T_f	15.094 °C	15.098 °C	15.104 °C
Mixture** Total E_f	-2.37 × 10^6 J	-2.31 × 10^6 J	-2.051 × 10^6 J
Solid Total E_f	1.33 × 10^9 J	1.33 × 10^9 J	1.33 × 10^9 J
Mixture ΔT	-19.22 °C	-19.21 °C	-19.18 °C
Solid ΔT	0.094 °C	0.098 °C	0. 104 °C

Mixture ΔE	-1.13 × 10^5 J	-5.49 × 10^4 J	2.05 × 10^5 J
Solid ΔE	4.025 × 10^5 J	4.215 × 10^5 J	4.462 × 10^5 J
Liquid Water Generated	121 g	117 g	100 g

*Solid is used to refer to both the soil and pipe together.

**Mixture refers to all phases in the fluid domain, gaseous phase and liquid phase. Gaseous phase is humid air (water vapor and dry air) and liquid phase is liquid water.

As the data in Table 4.2 show, the circulation of the hot humid air through the pipe led to the temperature drop in the mixture, temperature rise in the solid, and the condensation of water vapor (liquid water generation). For fan pressure jumps of 30Pa and 60Pa, the final energy of the mixture is smaller than the initial value, but for the fan pressure jump of 120Pa this is not the case and final state of the mixture has more energy than the initial state. This could be related to the thermal interactions between the liquid and gaseous phases within the mixture, or other factors (e.g. a source of error), but as mentioned before, due to the limitations of the Mixture multiphase model, the reason for this difference cannot be tracked with certainty. Compared to the case of dry air, humid air contains more energy and therefore took longer to reach its thermal equilibrium point with the solid. The data also show that greater fan velocities have led to higher final temperatures in the solid zone. A negative correlation is observed between the mass of the generated liquid water and the value of fan velocity (less water liquid is generated for greater fan velocities). Figure 4.5 shows the changes in average temperatures of a) the mixture and b) the soil. The mass of liquid water (solid lines, left ordinate) and the changes in the rate of liquid water production (solid lines with dots —●— right ordinate) are also shown in Figure 4.5 c).

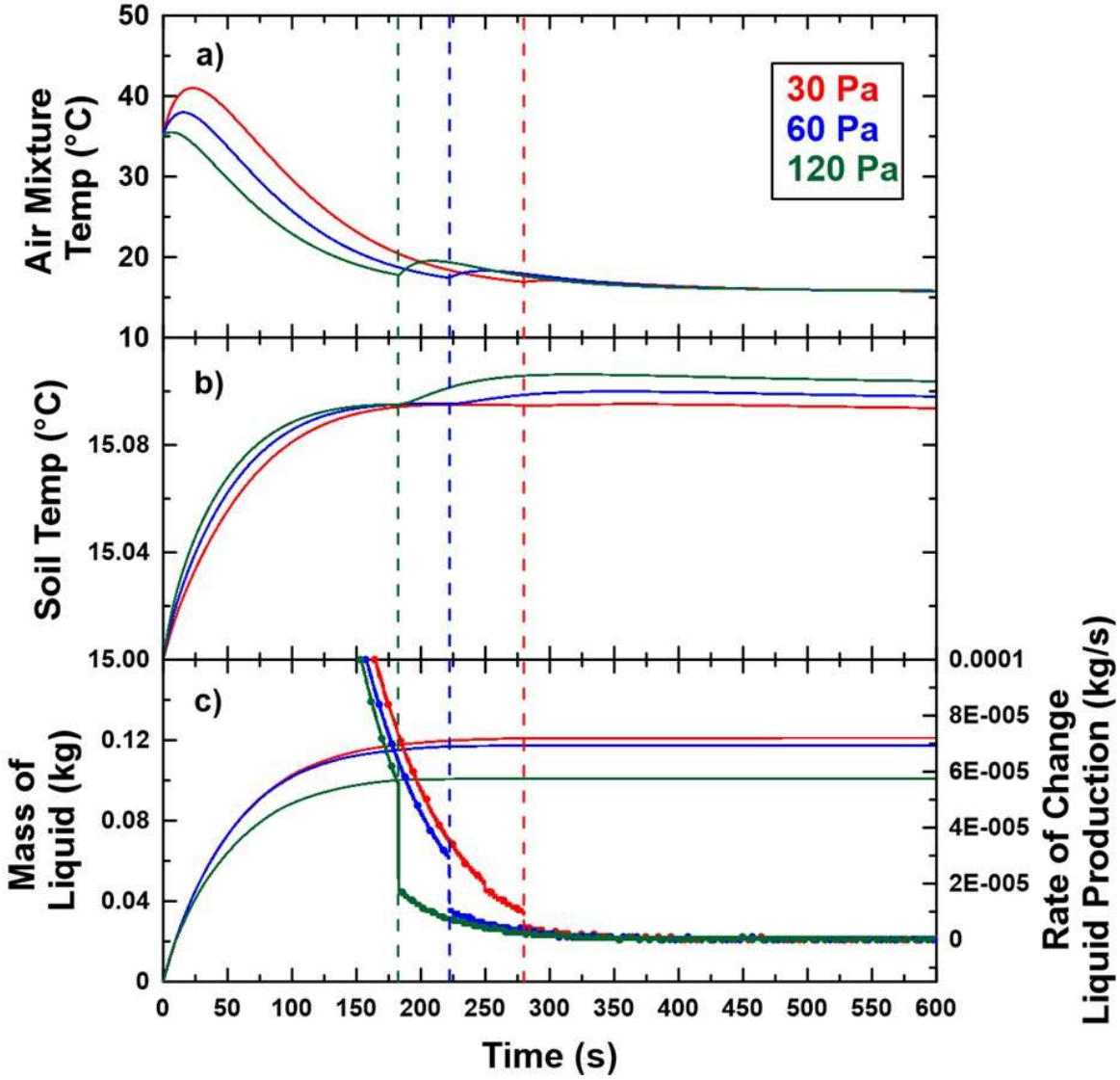

Figure 4.5: a) Change of the air mixture temperature over time, b) change of the soil temperature over time, c) mass of liquid water over time (solid lines, left ordinate) and rate of change in liquid water production over time (solid lines with dots —●— , right ordinate).

As shown in Figure 4.5 a), for all values of fan pressure jump, the temperature of the mixture initially rises and then decreases after a time Δt. Later, there is once again a small increase in the temperature for all three fan velocities after which the curves gradually become flat (indicating that thermal equilibrium between the mixture and the solid is reached). During the last 150 seconds of the simulation, all three curves are near horizontal indicating there is no change in the average temperature of the mixture. An inverse correlation is observed between the value of the fan pressure jump and the length of the time interval Δt indicating that Δt is shorter for higher fan pressure jumps and longer for lower fan pressure jumps. This rising and lowering of the mixture temperature is not known for certain however one possible explanation can be related to the generation of liquid water in the fluid domain. Condensation of water vapor will release latent heat which can be absorbed not only by the solid, but also by the air, which could increase the average temperature of the mixture. As time passes, circulation of the fluid as well as a drop in the rate of the liquid water generation, would end the energy absorption by air and thus the mixture temperature would begin to fall. As mentioned previously, increasing the fan velocity causes Δt to decrease. This supports the possibility of the fan velocity being one of the factors involved in the initial rise and fall of the mixture temperature. It would be of interest to see if a fan pressure jump smaller than 30PA (red-colored curve in Figure 4.5 a)) would result in a sharper initial rise in the average mixture temperature and if a fan pressure jump greater than 120PA (green-colored curve in Figure 4.5 a)) would result in a smaller

initial rise in average mixture temperature. Another possibility for the initial behavior of the mixture temperature could be the initial temperature of the liquid water, just after its generated in the fluid domain. If the generated liquid water was at a temperature greater than 35 °C, it would increase the average mixture temperature, only during the first few seconds of the simulation time but not after that (because of two reasons: first, after a few seconds the temperature of air has dropped enough to dominate the temperature rise imposed by liquid water, and second, the circulation of the fluid would transfer energy from the mixture to the soil reducing the average mixture temperature).

There is another kink (a rise followed by a fall) in all three curves of Figure 4.5 a) which is clearly related to the end of the generation of liquid water. Figure 4.5 c) shows the mass of liquid water (solid line, left ordinate) and the rate of change of liquid water production (solid lines with dots —●—, right ordinate) in the fluid domain for all fan velocities. Comparing Figures 4.5 a) and c) indicates that the rise in the mixture temperature shown in Figure 4.5 a) starts at the time that the rate of change in the liquid water production (Figure 4.5 c)) falls to its minimum value. It can also be observed that in Figure 4.5 a), lower fan pressure jumps led to a greater "initial rise" (during first 30 seconds) and smaller "second rise" (between t = 180s and t = 300s).

Figure 4.5 b) shows that, for all three fan velocities, the changes in average temperature of the solid (soil and pipe) follows a common pattern in which the temperature initially rises monotonically before becoming stable for a short period of time followed by another rise with a gradual decline. Same as the simulations involving dry air, it is observed that higher values of pressure jump cause the temperature to initially increase at a higher rate.

It was mentioned previously that conducting simulations with dry air could provide comparison to the present case with humid air. For hot humid air and cold solid, the generation of liquid water stops (water vapor content reaches a minimum equal to zero or very close to zero). At this point, if the average temperature of the mixture (dry air and liquid water) is still higher than the average temperature of the solid, then the process of heat transfer from the hot mixture to the cold solid should continue and a same pattern of change of the solid temperature is expected to be repeated. In Figure 4.5 c), the solid curves indicating the production of liquid water becomes flat and the curves indicating the rate of change of the production of water fall to their minimum values at times around t = 180s, 220s and 260s, for pressure jumps of 120Pa, 60Pa and 30Pa respectively. At these points, according to Figures 4.5 a) and b), the average temperature of the mixture is still more than the average temperature of the solid. Therefore, from these points on, "the temperature of the cold solid interacting with the hot mixture" is expected to change in the same way as the temperature of the cold solid increases after interacting with hot dry air. In other words, [at the times around t = 180s, 220s and 260s, for pressure jumps of 120Pa, 60Pa and 30Pa respectively], the curves in Figure 4.4 b) repeat the same pattern observed in Figure 4.3 b), where an initial rise is followed by a gradual fall. The difference, however, is that the rise and fall patterns in Figure 4.5 b) are less dramatic compared to those observed in Figure 4.3 b) which may be a result of the temperature difference between the hot mixture and the cold solid at the aforementioned times which is smaller than the temperature difference between hot dry air and cold soil at t = 0s.

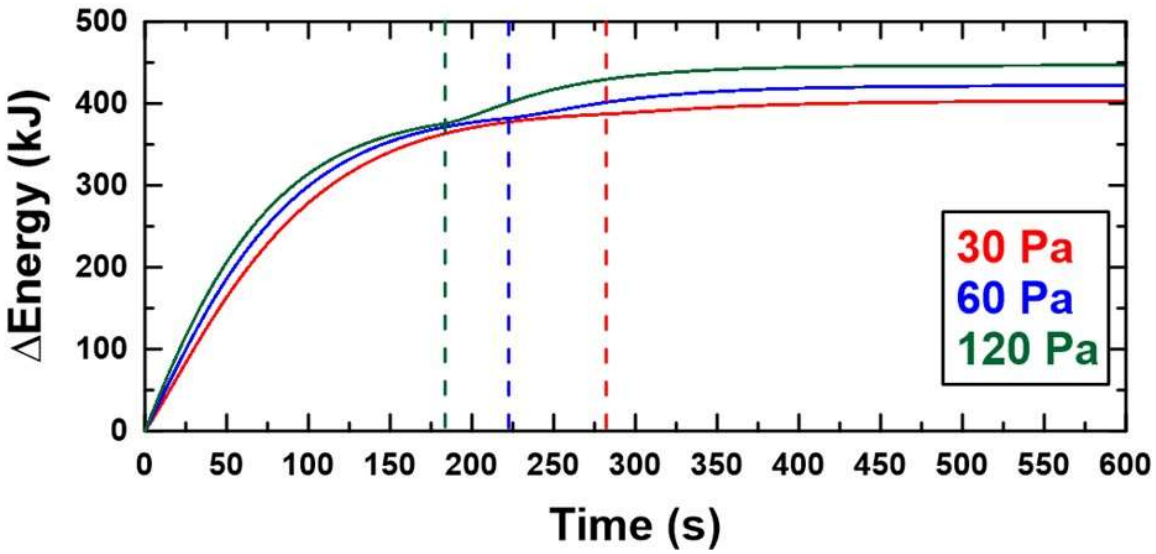

Figure 4.6: a) The change in energy of the soil for the three fan pressures (30 Pa (red), 60 Pa (blue), 120 Pa (green)).

Figure 4.6 shows the change in energy of the solid as a function of time for the three fan pressures considered in this work. It can be observed that all three curves increase monotonically before they undergo a transition (at the vertical dotted lines) where they rise again monotonically until they level off. The curves in figure 4.6 follow the same pattern as those shown in Figure 4.5 b) indicating an increase in energy of the soil due to the simultaneous condensation of moist air into liquid water and from the thermal contact of the warm air with the pipes in the soil. At the points indicated by the dotted lines where little humidity is left in the air the ground continues to absorb thermal energy from the warm air as it continues to flow in the pipes in the ground up to about 400s second when all three systems seem to have reached thermal equilibrium.

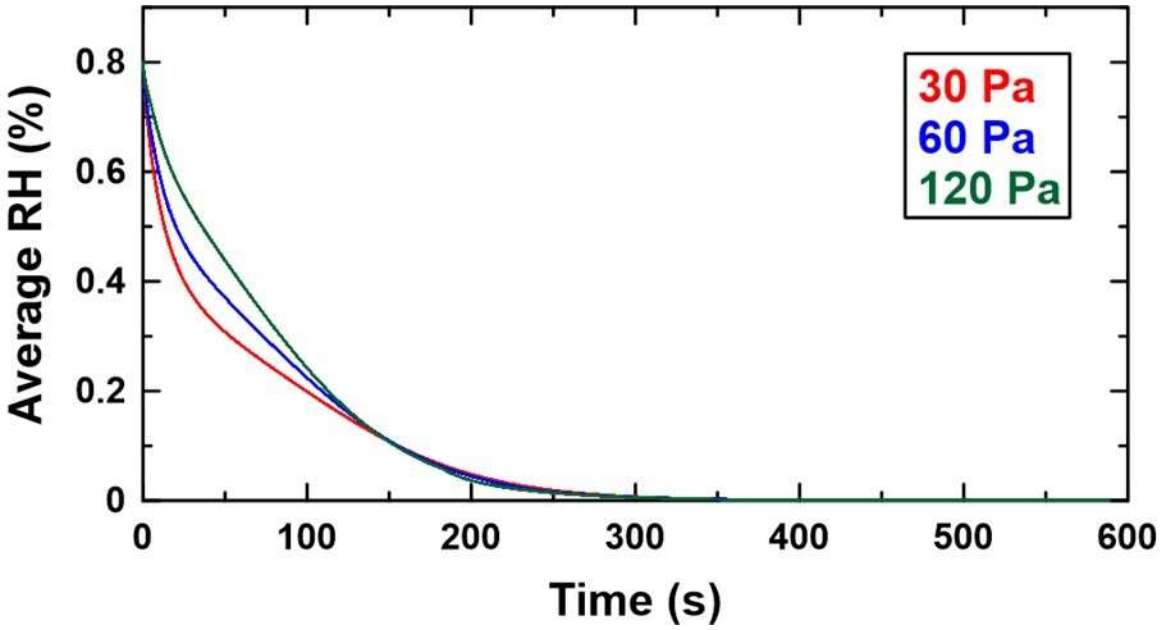

Figure 4.7: Changes in air average RH over time.

As the data in Table 4.2 showed, the circulation of hot humid air through a cold solid resulted in the generation of liquid water and the reduction of the RH in the air. The change in the average RH over time is shown in Figures 4.7 for all three fan pressure jump values.

Figure 4.7 shows that, for the first 15 seconds of the simulation time, the lower fan pressure jumps led to a faster change in average RH, meaning that the change in average RH occurred faster at 30Pa than of at 60Pa and 120Pa. As shown in Figure 4.5 a), during the first 15 seconds of the simulation time, lower fan pressure jumps correspond to a greater rise in mixture temperatures, which means the fall in the RH will occur at higher rate.

4.4.2.2 Cold Humid Air and Hot Soil

For this part, the goal was to investigate the processes which happen in the computational domain when cold air is circulated through warm solid. It was also intended to make the initial state of the domain as similar as possible to the final state of the domain from the previous part, except the temperature of the mixture. The initial temperature of the solid zones was selected to be the same as the final average temperature of the solid zone in the previous part (around 15 °C). In other words, the solid heated by the circulation of hot humid air in the previous part (e.g. daytime), was selected as a heat source to heat up the cold air at 5 °C and 50% RH (e.g. nighttime). To make the initial conditions of this part closer to the final conditions of the previous part, the amount of liquid water present in the fluid domain in the final state of the simulations of the last part were also added to the fluid domain for this part. Therefore, in addition to the cold relatively humid air (at 5 °C and 50% RH), liquid water was also present in the fluid domain. In summary: a mixture of 50% RH humid air and liquid water both at an average temperature of 5 °C was circulated through the warm solid. The results of these simulations for three different fan pressure jump values are presented in Table 4.3.

Table 4.3: Results of simulations conducted when cold humid air initially set to 5 °C and 50% RH was circulated through a pipe surrounded by soil with an initial temperature of around 15 °C for 200s.

Fan Pressure Jump	30Pa	60Pa	120Pa

Mixture** T_i	5 °C	5 °C	5 °C
Air RH_i	50%	50%	50%
Initial Mass of Liquid Water	121 g	117 g	100 g
Solid* T_i	15.094 °C	15.098 °C	15.104 °C
Mixture Total E_i	-2.69×10^6 J	-2.63×10^6 J	-2.37×10^6 J
Solid Total E_i	1.33×10^9 J	1.33×10^9 J	1.33×10^9 J
Fan Velocity in Y Axis Direction	-5.91 m/s	-8.43 m/s	-12.05 m/s
Mixture Avg T_f	15.89 °C	15.90 °C	15.79 °C
Air RH_f	0.26%	0.30%	0.28%
Solid* Avg T_f	15.09 °C	15.10 °C	15.11 °C
Mixture Total E_f	-2.64×10^6 J	-2.56×10^6 J	-2.27×10^6 J
Solid Total E_f	1.33×10^9 J	1.33×10^9 J	1.33×10^9 J
Mixture ΔT	10.89 °C	10.90 °C	10.79 °C
Solid ΔT	-0.0005 °C	0.002 °C	0.008 °C
Mixture ΔE	4.92×10^4 J	6.67×10^4 J	9.98×10^4 J
Solid ΔE	-5×10^3 J	6×10^3 J	28×10^3 J
Final Mass of Liquid Water	133 g	129 g	110 g

*Solid is used to refer to both soil and pipe together.

**Mixture refers to all phases in the fluid domain, gaseous phase and liquid phase. Gaseous phase is humid air (water vapor and dry air) and liquid phase is liquid water.

As the data in Table 4.3 show, the circulation of the cold humid mixture through the pipe embedded inside the warm soil led to a considerable rise in the mixture temperature and the condensation of water vapor (liquid water generation). For fan pressure jumps of 120Pa and 60Pa, the solid zones showed higher final temperatures (and energies as well). Nevertheless, for the 30Pa fan pressure jump, the solid zone lost energy and suffered a tiny drop in the average temperature, which, as discussed before, is due to the limitations of the Mixture multiphase model and cannot be tracked confidently. Figure 4.8 shows the change in average temperature of the a) mixture and b) solid. The mass of liquid water (left side) and the rate of change in the liquid water production (right side) are also shown in Figure 4.8 c).

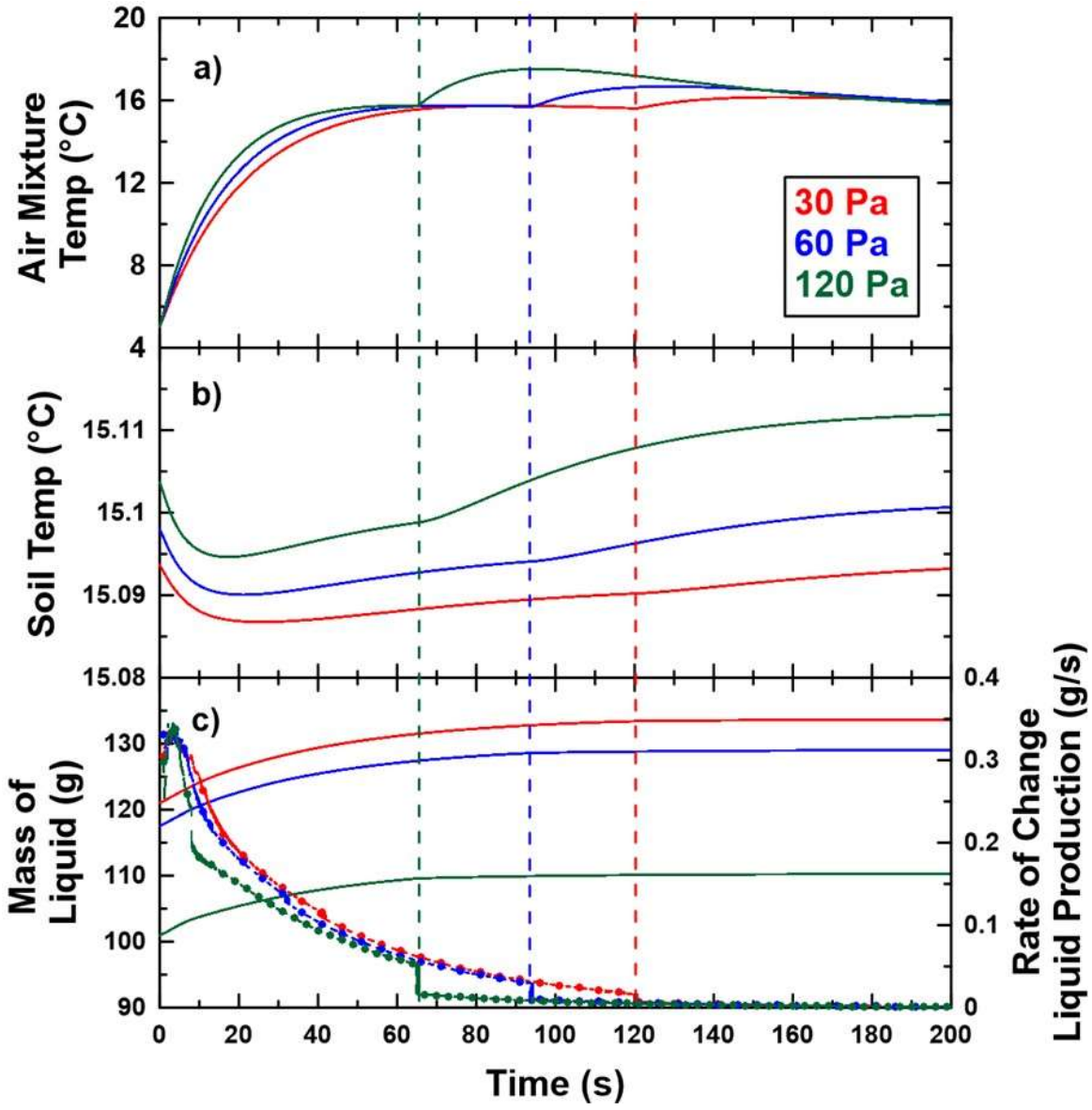

Figure 4.8: a) Changes of air mixture temperature over time. b) Changes of soil temperature over time. c) Mass of liquid water over time (left) and rate of change in liquid water production over time (right).

Figure 4.8 a) shows that for all three fan pressure jumps, the average mixture temperature initially rises and then becomes stable for a short period of time before it undergoes another rise which then gradually decreases. Comparing Figures 4.8 a) and the data shown by the left ordinate of 4.8 c) (solid lines with dots —●—) suggests that the temperature of the mixture becomes almost flat at points where the curves representing the mass of the liquid water become flat. In other words, the mixture temperature becomes stable at the same time as the generation of liquid water (condensation of water vapor) in the domain ends. Then, the temperature rises again, reaches a maximum value and after that gradually declines. An interesting comparison can be made here between the behavior patterns of the solid temperature in section 4.4.2.1 (Figure 4.5 b)) and mixture temperature in section 4.4.2.2 (Figure 4.8 a)). In the latter case, the cold mixture is thermally interacting with the warm solid, and in the former, the cold solid was thermally interacting with the hot mixture. The common pattern observed by both is that temperature is initially rising and becomes stable for a short period of time [this is the point at which generation of liquid water ends in both cases], then another rise followed by a fall. The difference, however, is that for the mixture temperature (Figure 4.8 a)) the fall at the end is more dramatic than for the solid temperature (Figure 4.5 b)). This is because of two reasons: First, the mass of soil domain is much greater than the mixture, and second, the specific heat of the mixture is around 30% less than the specific heat of soil. Therefore, under similar conditions, the average temperature of the mixture declines faster than the average temperature of soil.

Figure 4.8 b) illustrates the changes in the solid average temperature for three fan velocities. The average temperatures are initially falling for a short period of time, then rising in a

two-step process until the end of simulation time. The temperatures are initially decreasing, since the solid is warmer than the mixture. After a time span of Δt is passed, the temperatures can be seen rising. There is a change in the rate for all the fan velocities which is coincident with the mass of liquid water becoming stable (Figure 4.8 c) left-ordinate) and the rate of liquid water production dropping (Figure 4.8 c) right-ordinate). In other words, the average temperature of the solid is rising (Figure 4.8 b)) when the generation of liquid water ends (curves becoming flat in Figure 4.8 c) left-ordinate). Shortly after that point, an increase in the rate of the solid temperature is observed (slopes become steeper in Figure 4.8 b)). Following this the rate of change in the temperature decreases as the simulation proceeds to the end (t = 200s) and the temperature of the solid becomes stable.

The left ordinate of Figure 4.8 c) shows the change in the mass of liquid water in the fluid domain for three fan velocities. It can be observed that, after the simulation begins, the mass of liquid water starts rising (indicating that condensation is taking place) after which the curves gradually become flat (which means condensation has stopped and the mass of liquid water is not changing). This case is demonstrating the thermal interactions between warm soil (initially at 15 °C) and cooler humid air (initially at 5 °C and RH of 50%). Initially, the direction of heat transfer is from the warmer soil to colder air as indicated by Figures 4.8 a) and b) showing the temperature of air increasing and temperature of soil decreasing. The direction of heat transfer from the soil to the air might make condensation unexpected, but it should be noted that the saturation temperature of water vapor (the temperature at which vapor starts condensing into liquid) is a function of pressure and does not merely depend on the direction of heat transfer between the soil and air. Therefore, in

this case, although the soil is initially losing energy while the mixture is gaining energy, condensation of the vapor in the humid air is also occurring resulting in the production of liquid water.

The left ordinate in Figure 4.8 c) also shows that all three curves follow the same pattern where initially they increase slightly followed by a steep decrease until after a time Δt where they become flat (condensation ends). The length of time Δt is shorter for higher fan velocities because the circulation flow at higher speed means a higher rate of mass [and heat] transfer, which subsequently means condensation happens at a higher rate (which depletes the vapor content in the humid air faster).

Figure 4.9 shows the change in energy of the solid as a function of time for the three fan pressures considered in this work. It can be observed that all three curves follow the same pattern in which the soil initially loses energy and after some time begins to gain energy. We believe that there three thermal processes occurring at the same time which are affecting the energy of the soil. Initially the warmer soil is losing energy to the colder air as the latter is flowing through the pipe. Also, initially for times on the right of the dotted lines, the soil is also gaining energy from the condensation of liquid in the pipe as was also observed in the previous section. Lastly, the soil is also absorbing thermal energy due to the moving gas in the pipe. According to the kinetic theory of gases, when the fan circulates the air in the pipe it produces thermal energy equal ½ $k_B T$ for every degree of freedom and for every air molecule in the fluid. For this two-dimensional case this gives a thermal energy $E_T = Nk_B T$. Assuming the air in the fluid behaves like an ideal gas allows us to solve for the number of gas molecules $N = PV/k_B T$ giving the thermal energy of the gas in the pipe to be

on the order of $E_T = PV \approx 15$ kJ of which some of it is continuously being injected into the soil. The greater the fan pressure value the more thermal energy the gas has which explains why the 120Pa data shows a larger increase in soil energy than the 30 Pa data. It should also be noted that these changes in energy are small compared to those observed in section 4.4.2.

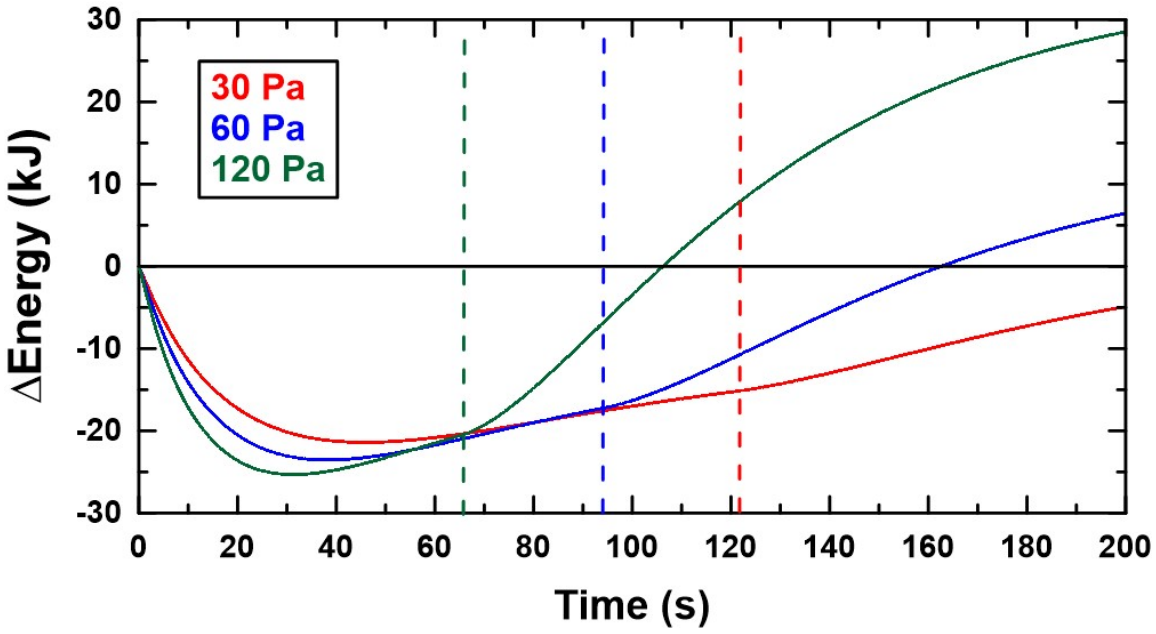

Figure 4.9: The change in energy of the soil for the three fan pressures (30 Pa (red), 60 Pa (blue), 120 Pa (green)).

As the data in Table 4.3 show, the circulation of cold relatively humid mixture through a warm solid resulted in the generation of liquid water in the fluid domain and the reduction

of the RH in the gaseous phase of the mixture. The changes in average RH over time are shown in Figure 4.10.

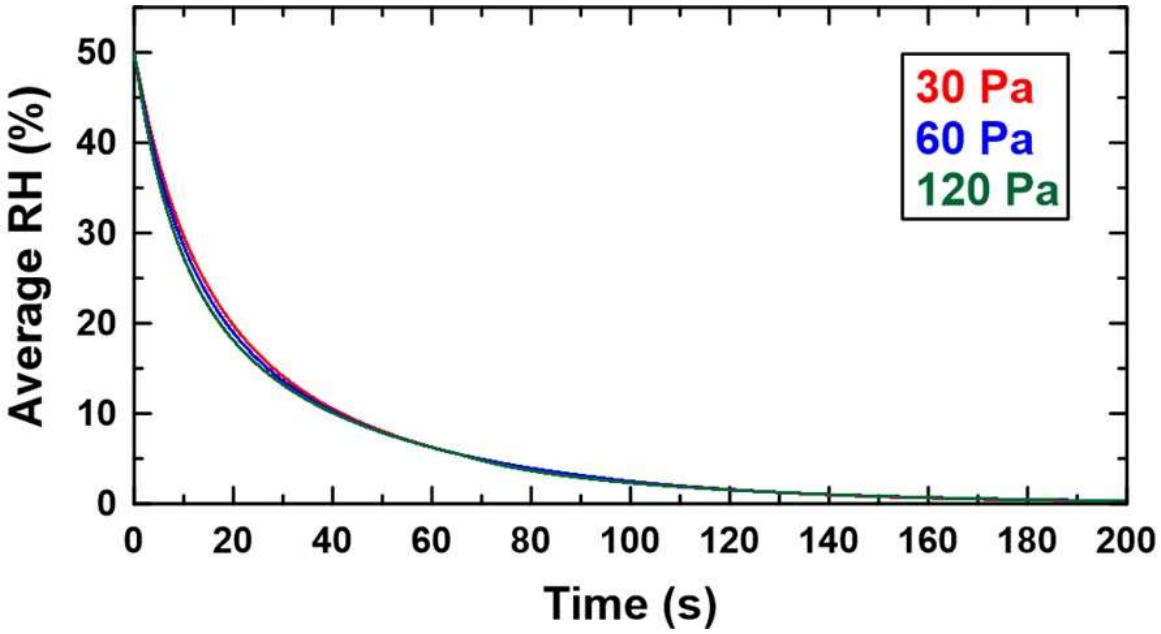

Figure 4.10: Changes in air average RH over time.

Figure 4.10 illustrates the changes in the average RH of humid air. The same behavior pattern is observed in all three curves. As the simulation proceeds the slope of the curves decreases indicating a decrease in the rate at which RH is dropping. This is because the temperature of air is rising and the vapor content is decreasing, so the RH decreases at a lower rate.

In the next chapter, the conclusion of this work as well as suggestions for further research will be presented.

Chapter 5 Conclusions and Potential for Future Research

5.1 Conclusions

The main objective of this work was to develop the computational knowhow using ANSYS Fluent to model the heat transfer process of four-season greenhouses in an attempt to one day be able to optimize the design of the GAHT system. Four possible modelling scenarios were considered:

1. Model the air flow and condensation using one of the available multiphase models with soil as a porous medium.
2. Model the air flow with wall condensation using the Eulerian Wall Film model with soil as a solid material (in 3D).
3. Model the air flow and condensation using the Mixture multiphase model with soil as a solid material (in 2D).
4. Model the air flow and condensation using the Mixture multiphase model with soil as a solid material (in 3D).

In scenario number 1, a limitation was imposed by the software in that multiphase flows could be modeled in porous regions only when there is thermal equilibrium between the flow and the solid structure of the porous region. This meant that no heat transfer between the soil and the flow of humid air could be included in the calculations, and since heat transfer is the central core of GAHT systems, this scenario was not selected. Scenarios number 2 and 4 were tested for short simulation times and converged solutions were

achieved for both. However, meshes of 3D geometries had very high element numbers which led to the solutions requiring extremely long time to complete making the computations costly. Therefore, no further simulations were conducted for these two scenarios. Scenario number 3, which is a 2D variation of scenario number 4, was finally selected for conducting simulations under different boundary conditions. In order to increase the accuracy of the Mixture multiphase model for modeling phase changes, a UDF was written and compiled with the software. This UDF calculates the saturation temperature of vapor, at which condensation takes place, based on the partial pressure of the water vapor.

Circulation of the air flow through the soil and the processes which occur as a result of it were simulated for three situations: hot dry air and cold soil, hot humid air and cold soil, and cold humid air and warm soil. To study the effect(s) of the fan velocity on the results, all simulations were conducted for three different fan velocities.

Results of circulating hot dry air through colder soil showed that the transfer of thermal energy from the air to the soil occurs relatively fast, resulting in a significant temperature drop in the air and a minor temperature increase in the soil. A positive correlation between the fan velocity and rate of change in the temperature was observed (especially at early times in the simulations where the temperature difference between the air and the solid was a maximum). In other words, higher fan velocities led to faster temperature drops in the air and the temperature raise in the soil. The results of this part also showed that the amount of energy lost by the air was (with negligible error) equal to the amount of energy absorbed by the soil, thus satisfying the principle of conservation of energy. In the next part, humidity

was added to the air, resembling the air found inside a typical greenhouse. In this part, hot humid air was circulated through the colder soil which resulted in the transfer of thermal energy from the air to the soil as well as the generation of liquid water. The results of this part demonstrated the capability of soil for use as a thermal energy storage medium for excess heat which exists in the greenhouses' air during daytime. At the end of the simulations for this part, due to the heat transfer from the air to the soil, the air temperature was regulated, and the temperature and internal energy of the soil were increased. The soil's final state in this part was then taken as the initial state of the soil for the last part where relatively humid cold air was circulated through the warmer soil. The results of this last part showed that the soil can be used as an energy source to heat the greenhouses' cold air and raise its temperature during the nighttime. When the last two parts take place successively, they form a cycle in which (during the day) excess heat in the air is transferred to the soil and stored there, resulting in the regulation of the air temperature without using external cooling systems and preventing the energy from being wasted. Later (during the night), when the greenhouse air temperature is likely to drop below a suitable value, the soil is used as a heat source to raise the air temperature without requiring an external heating system. This approach demonstrated great potential in the way of cutting or minimizing the need for external heating/cooling systems in greenhouses and making them more energy efficient.

5.2 Suggestions for Future Works

ANSYS Fluent proved to be a powerful and accurate simulation tool with various options which enables researchers to model and study different phenomena. The software benefits from several features which can be utilized in future work in the field of four-season greenhouses. The recommendations for further research can be made with regards to the different aspects of the GAHT system tested in this work:

5.2.1 Initial Conditions

In the calculations involving humid air, our simulations went from a daytime scenario straight to a nighttime scenario in which the soil was loaded with energy and used as a heat source to increase the temperature of the cold nighttime air inside the greenhouse (initially at 5 °C for nighttime scenario). In reality the temperature inside a typical greenhouse slowly decreases as daytime turns into night. In future calculations, different initial temperatures of air (as well as soil) can be used, to investigate the limits of the thermal storage capacity of soil. For example, simulations can be conducted with the initial air temperature inside the greenhouse decreasing from 30 °C to -20 °C in increments of 5 °C.

5.2.2 Regarding the External Factors

One of the software's built-in features is the "solar simulator" which allows the user to include the thermal effects of the sun's radiation in their modeling and simulations. As discussed in chapter 2, solar radiation can significantly affect the overall performance of the greenhouse. Including the effects of solar illumination should make the simulations and their results more realistic and comprehensive. Including the effects of solar radiation into

the model could potentially allow the various properties (radiometric, thermal, and mechanical) of the covering materials to be considered. Thus, modeling and testing the behavior of different covering materials under certain solar radiation and for different latitudes is another recommendation for future research concerning the external factors affecting the overall performance of four-season greenhouses.

5.2.3 Regarding the Internal Factors

The phase change of humid air is a subject for further and deeper examination. Among the three multiphase models included in ANSYS Fluent, Volume of Fluid (VOF), Mixture, and Eulerian, the Eulerian model is the only one which solves a separate set of momentum and energy equations for each phase (in this case air and liquid water). The mixture multiphase model solves only one set of momentum (and energy) equations for the mixture as a whole and calculates bulk temperature and bulk energy of the mixture. As discussed in chapter 4, when using the Mixture multiphase model, it is not possible to track the interactions between gaseous and liquid phases taking place within the mixture. The Eulerian multiphase model solves *n* sets of momentum (and energy) equations for *n-phases* of the mixture. Therefore, modeling phase changes using this model would be an interesting suggestion for future work. This model enables the user to track gaseous and liquid phases separately, thus providing more maneuverability in studying the behaviors of air and liquid water separately, as well as their interactions with each other.

In this work, to model the condensation of water vapor, a UDF was written and compiled with Fluent. This UDF was written according to the Antoine equation, one of the several semi-empirical correlations describing the relationship between saturation temperature and

the vapor pressure. In future work, this UDF can be written according to other available models and tested in simulations.

The effects of interactions between the plants, environment, and the greenhouse structure can influence the energy consumption and crop yield [21]. Therefore, another recommendation for future research concerning the effects of internal factors would be attempting to include the thermal effects of the plants inside the greenhouse by introducing energy sources/tanks. The soil domain, used as a heat storage in this work, can also be replaced by another material, e.g. a large tank of water, which will then be heated by the hot air (daytime) and used as an energy source to heat up the air (nighttime).

5.2.4 Regarding the Geometry Design

Different geometries for the GAHT system can be tested in future research, such as: variations of pipe size and placement, different ratios of chamber to soil volumes, etc. For instance: how would the performance of the system be affected by implementing two lines of pipe (instead of one) passing through the soil beneath the chamber? Or, how would the system behave if the volume of fluid domain was doubled?

Instead of putting the pipe in direct contact with the soil, what if the solid pipe was replaced with a perforated pipe with a very porous material placed between the pipe and the soil. In other words, how would a “perforated pipe surrounded by a very porous material and embedded under soil” affect the process of heat transfer? For this instance, another CFD simulation tools would need to be used since in ANSYS Fluent, as of 2024, none of

multiphase models are compatible with non-equilibrium thermal modeling for porous media.

In chapter 4 section 4.4.2.1, it was shown in Figure 4.4 a) that, when hot humid air is circulated through the cold soil, the average temperature of the air initially increased before decreasing again (for example at around t = 30s for the 30Pa fan pressure jump). Figure 5.1 shows the temperature map of the system at t = 30s. It can be observed that the temperature of air reached values around 45 °C at the center of the greenhouse chamber. This indicates that, because of the laminar flow of the air, a considerable amount of heat at the center of the chamber is not being accessed. Future work could involve creating turbulent flow in the central area of the chamber to access more of the available heat in the air.

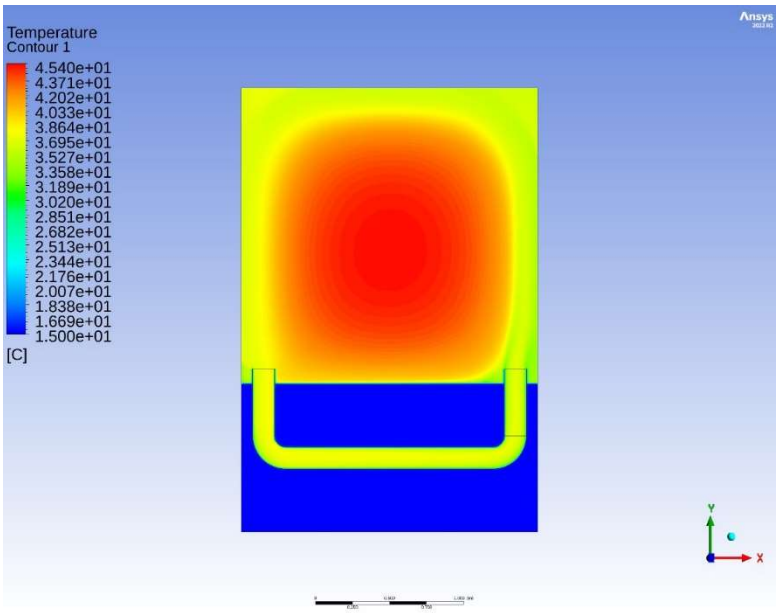

Figure 5.1: Map of temperature distribution at t = 30s during the circulation of hot humid air (initially at 35 °C and 80% RH) through the cold soil (initially at 5 °C) at 30Pa fan pressure jump.

References

1. Wittwer, Sylvan H. and Nicolás Castilla. “Protected Cultivation of Horticultural Crops Worldwide.” Horttechnology 5.1 (1995): 6-23.
2. Tiwari, G. N.. Greenhouse Technology for Controlled Environment. India, Alpha Science, 2003.
3. Rajesh, T., et al. "Chapter-1 Plant Protection using Cold Frame." *Chief Editor Dr. Varsha Rani* 103 (2020): 1.
4. Yoon, Sang Jun, and Jan Woudstra. “Advanced Horticultural Techniques in Korea: The Earliest Documented Greenhouses.” *Garden History*, vol. 35, no. 1, 2007, pp. 68–84. *JSTOR*, http://www.jstor.org/stable/25472355. Accessed 10 May 2024.
5. Young, Terence. “From Manure to Steam: The Transformation of Greenhouse Heating in the United States, 1870-1900.” *Agricultural History*, vol. 72, no. 3, 1998, pp. 574–96. *JSTOR*, http://www.jstor.org/stable/3744571. Accessed 12 May 2024.
6. Schiller, Lindsey. The year-round solar greenhouse: how to design and build a net-zero energy greenhouse. New Society Publishers, 2016.
7. Rorabaugh, P., M. Jensen, and Gene Giacomelli. "Introduction to controlled environment agriculture and hydroponics." Control. Environ. Agric. Cent (2002): 1-130.
8. Noureddine Choab, Amine Allouhi, Anas El Maakoul, Tarik Kousksou, Said Saadeddine, Abdelmajid Jamil, Review on greenhouse microclimate and application: Design parameters, thermal modeling and simulation, climate controlling technologies, Solar Energy, Volume 191, 2019, Pages 109-137, ISSN 0038-092X,https://doi.org/10.1016/j.solener.2019.08.042. (https://www.sciencedirect.com/science/article/pii/S0038092X19308205).
9. D. Briassoulis, D. Waaijenberg, J. Gratraud, B. von Eslner, Mechanical Properties of Covering Materials for Greenhouses: Part 1, General Overview, Journal of Agricultural Engineering Research, Volume 67, Issue 2, 1997, Pages 81-96, ISSN

0021-8634,https://doi.org/10.1006/jaer.1997.0154. (https://www.sciencedirect.com/science/article/pii/S0021863497901542).

10. G. Papadakis, D. Briassoulis, G. Scarascia Mugnozza, G. Vox, P. Feuilloley, J.A. Stoffers, Review Paper (SE—Structures and Environment): Radiometric and Thermal Properties of, and Testing Methods for, Greenhouse Covering Materials, Journal of Agricultural Engineering Research, Volume 77, Issue 1, 2000, Pages 7-38, ISSN 0021-8634, https://doi.org/10.1006/jaer.2000.0525. (https://www.sciencedirect.com/science/article/pii/S0021863400905250).
11. V.P. Sethi, On the selection of shape and orientation of a greenhouse: Thermal modeling and experimental validation, Solar Energy, Volume 83, Issue 1, 2009, Pages 21-38, ISSN 0038-092X, https://doi.org/10.1016/j.solener.2008.05.018. (https://www.sciencedirect.com/science/article/pii/S0038092X08001540).
12. Hassan Ghasemi Mobtaker, Yahya Ajabshirchi, Seyed Faramarz Ranjbar, Mansour Matloobi, Simulation of thermal performance of solar greenhouse in north-west of Iran: An experimental validation, Renewable Energy, Volume 135, 2019, Pages 88-97, ISSN 0960-1481, https://doi.org/10.1016/j.renene.2018.10.003. (https://www.sciencedirect.com/science/article/pii/S096014811831187X).
13. Mathala J Gupta, Pitam Chandra,Effect of greenhouse design parameters on conservation of energy for greenhouse environmental control, Energy, Volume 27, Issue 8, 2002, Pages 777-794, ISSN 0360-5442, https://doi.org/10.1016/S0360-5442(02)00030-0. (https://www.sciencedirect.com/science/article/pii/S0360544202000300)
14. Kumari, Nisha, G. Tiwari, and M. Sodha. "Performance evaluation of greenhouse having passive or active heating in different climatic zones of India." (2007).
15. Murat KACIRA, Sadanori SASE, Limi OKUSHIMA, Effects of Side Vents and Span Numbers on Wind-Induced Natural Ventilation of a Gothic Multi-Span Greenhouse, Japan Agricultural Research Quarterly: JARQ, 2004, Volume 38, Issue 4, Pages 227-233, Released on J-STAGE February 27, 2014, Online ISSN 2185-8896, Print ISSN 0021-

3551, https://doi.org/10.6090/jarq.38.227, https://www.jstage.jst.go.jp/article/jarq/38/4/38_227/_article/-char/en.

16. Karlos Espinoza, Alejandro López, Diego L. Valera, Francisco D. Molina-Aiz, José A. Torres, Araceli Peña, Effects of ventilator configuration on the flow pattern of a naturally-ventilated three-span Mediterranean greenhouse, Biosystems Engineering, Volume 164, 2017, Pages 13-30, ISSN 1537-5110, https://doi.org/10.1016/j.biosystemseng.2017.10.001. (https://www.sciencedirect.com/science/article/pii/S153751101730466X).
17. Chao Chen, Yin Li, Na Li, Shen Wei, Fengguang Yang, Haoshu Ling, Nan Yu, Fengtao Han, A computational model to determine the optimal orientation for solar greenhouses located at different latitudes in China, Solar Energy, Volume 165, 2018, Pages 19-26, ISSN 0038-092X, https://doi.org/10.1016/j.solener.2018.02.022. (https://www.sciencedirect.com/science/article/pii/S0038092X18301488).
18. Dragicevic, Snezana. (2010). Determining the optimum orientation of a greenhouse on the basis of the total solar radiation availability. Thermal Science - THERM SCI. 15. 57-57. 10.2298/TSCI100220057D.
19. Brun, R. and de Villele, O. (1974). ORIENTATION OF GREENHOUSES IN THE MEDITERRANEAN ZONE. Acta Hortic. 42, 43-54 DOI:10.17660/ActaHortic.1974.42.3 https://doi.org/10.17660/ActaHortic.1974.42.3
20. P.K. Sharma, G.N. Tiwari, V.P.S. Sorayan, Temperature distribution in different zones of the micro-climate of a greenhouse: a dynamic model, Energy Conversion and Management, Volume 40, Issue 3, 1999, Pages 335-348, ISSN 0196-8904, https://doi.org/10.1016/S0196-8904(98)00100-9. (https://www.sciencedirect.com/science/article/pii/S0196890498001009)
21. P.I. Cooper, R.J. Fuller, A transient model of the interaction between crop, environment and greenhouse structure for predicting crop yield and energy consumption, Journal of Agricultural Engineering Research, Volume 28, Issue 5, 1983, Pages 401-417, ISSN 0021-8634, https://doi.org/10.1016/0021-

8634(83)90133-6.
(https://www.sciencedirect.com/science/article/pii/0021863483901336)

22. T. Boulard, A. Baille, Analysis of thermal performance of a greenhouse as a solar collector, Energy in Agriculture, Volume 6, Issue 1, 1987, Pages 17-26, ISSN 0167-5826,https://doi.org/10.1016/0167-5826(87)90018-0.
(https://www.sciencedirect.com/science/article/pii/0167582687900180).
23. J.G. Pieters, J.M. Deltour, Modelling solar energy input in greenhouses, Solar Energy, Volume 67, Issues 1–3, 1999, Pages 119-130, ISSN 0038-092X, https://doi.org/10.1016/S0038-092X(00)00054-2.
(https://www.sciencedirect.com/science/article/pii/S0038092X00000542)
24. T. Boulard, C. Kittas, J.C. Roy, S. Wang, SE—Structures and Environment: Convective and Ventilation Transfers in Greenhouses, Part 2: Determination of the Distributed Greenhouse Climate, Biosystems Engineering, Volume 83, Issue 2, 2002, Pages 129-147, ISSN 1537-5110, https://doi.org/10.1006/bioe.2002.0114.
(https://www.sciencedirect.com/science/article/pii/S1537511002901145).
25. Hacene Bouhoun Ali, Pierre-Emmanuel Bournet, Patrice Cannavo, Etienne Chantoiseau, Development of a CFD crop submodel for simulating microclimate and transpiration of ornamental plants grown in a greenhouse under water restriction, Computers and Electronics in Agriculture, Volume 149, 2018, Pages 26-40, ISSN 0168-1699, https://doi.org/10.1016/j.compag.2017.06.021.
(https://www.sciencedirect.com/science/article/pii/S0168169916306883)
26. Xiangli He, Jian Wang, Shirong Guo, Jian Zhang, Bin Wei, Jin Sun, Sheng Shu, Ventilation optimization of solar greenhouse with removable back walls based on CFD, Computers and Electronics in Agriculture, Volume 149, 2018, Pages 16-25, ISSN 0168-1699, https://doi.org/10.1016/j.compag.2017.10.001.
(https://www.sciencedirect.com/science/article/pii/S0168169917303447).
27. Xiao-wei WANG, Jin-yao LUO, Xiao-ping LI, CFD Based Study of Heterogeneous Microclimate in a Typical Chinese Greenhouse in Central China, Journal of Integrative Agriculture, Volume 12, Issue 5, 2013, Pages 914-923, ISSN 2095-

3119, https://doi.org/10.1016/S2095-3119(13)60309-3. (https://www.sciencedirect.com/science/article/pii/S2095311913603093).

28. Davide Piscia, Juan I. Montero, Esteban Baeza, Bernard J. Bailey, A CFD greenhouse night-time condensation model, Biosystems Engineering, Volume 111, Issue 2, 2012, Pages 141-154, ISSN 1537-5110, https://doi.org/10.1016/j.biosystemseng.2011.11.006. (https://www.sciencedirect.com/science/article/pii/S1537511011002017).
29. Nebbali, R., Roy, J.C., Boulard, T. and Makhlouf, S. (2006). COMPARISON OF THE ACCURACY OF DIFFERENT CFD TURBULENCE MODELS FOR THE PREDICTION OF THE CLIMATIC PARAMETERS IN A TUNNEL GREENHOUSE. Acta Hortic. 719, 287-294 DOI:10.17660/ActaHortic.2006.719.32.https://doi.org/10.17660/ActaHortic.2006.719.32.
30. Bhaskaran, R., & Collins, L. (2002). Introduction to CFD basics. Cornell University-Sibley School of Mechanical and Aerospace Engineering, 1-21.
31. Malalasekera, W. (2007). An introduction to computational fluid dynamics: the finite volume method. Pearson Prentice Hall.
32. ANSYS Inc. ANSYS FLUENT User's Guide, Release 2022 R2.
33. ANSYS, Inc. (2009) ANSYS Fluent Theory Guide, Release 12.0.
34. Needelman, B. A. (2013) What Are Soils? Nature Education Knowledge 4(3):2
35. Antoine, C. (1888). Tensions des vapeurs; nouvelle relation entre les tensions et les temperatures. Comptes rendus hebdomadaires des séances de l'Académie des sciences, T 107, Pages: 681–684, 778–780, 836–837. (In French). (https://gallica.bnf.fr/ark:/12148/bpt6k30635?rk=42918;4).
36. Li, Dongqing. "Encyclopedia of Microfluidics and Nanofluidics." (2008).
37. Reddy, J. N. 2019. Introduction to the Finite Element Method. 4th ed. New York: McGraw-Hill Education. https://www.accessengineeringlibrary.com/content/book/9781259861901.
38. Fletcher, Clive. "Computational Galerkin Methods." (1983).

39. Xin-She Yang, Chapter 28 - Mathematical Modeling, Editor(s): Xin-She Yang, Engineering Mathematics with Examples and Applications, Academic Press, 2017, Pages 325-340, ISBN 9780128097304, https://doi.org/10.1016/B978-0-12-809730-4.00037-9.
(https://www.sciencedirect.com/science/article/pii/B9780128097304000379)

Appendix A

The Antoine equation is a semi-empirical formula used to express the relation between vapor pressure and the temperature at which vapor becomes saturated and condensation happens. The equation is given by:

$$log_{10}(p) = A - \frac{B}{C + T} \tag{A1}$$

Where p is the value of the vapor pressure in [mmHg], T is the value of the vapor temperature in [°C] and A, B, and C are unitless component-specific constants. The equation can also be represented in a temperature-explicit form with the proper constants. The temperature explicit form of equation A1 where p is the value of the vapor pressure in [Pa] and T is the value of the saturation temperature in [K] is given by the following [35]:

$$T = \frac{B}{A - log_{10}(p)} - C \tag{A2}$$

For water vapor within the range of $274.15\ K\ < T < 372.15\ K$, the A, B, and C constants are given by:

$A = 10.19621$

$B = 1730.63$

$C = 39.724$

The UDF used in this work, written according to Antoine's equation in the C programing language, was:

```
#include "udf.h"


DEFINE_PROPERTY(saturation_temperature,c,t)
{
    real sat_temp;//saturation temperature of humid air containing dry air and water vapor.
    real vapor_p;//pressure of vapor.
    real static_p = C_P(c,t);//static pressure.
    real operating_p = RP_Get_Real("operating-pressure");//operating pressure.
    vapor_p = static_p + operating_p;//vapor pressure is sum of static and operating pressures.
    sat_temp = (1730.63/(10.19621 - log10(vapor_p))) - 233.426 + 273.15;//Antoine equation.
    return sat_temp;
}
```